MEASUREMENT OF ALTERNATING CURRENT LOSSES IN HIGH-T_c SUPERCONDUCTORS

Thesis

Submitted to

Graduate Engineering and Research

School of Engineering

UNIVERSITY OF DAYTON

In Partial Fulfillment of the Requirements for

The Degree

Master of Science in Electro-Optics

by

Kamal Kanti Das

UNIVERSITY OF DAYTON

Dayton, Ohio

May 1994

MEASUREMENT OF ALTERNATING CURRENT LOSSES IN HIGH-T_c SUPERCONDUCTORS

APPROVED BY:

Binod Kumar, Ph.D.
Associate Professor, Electro-Optics
Advisory Committee, Chairperson

Mohammad A. Karim, Ph.D.
Director, Electro-Optics Program
Committee member

Gordon R. Little, Ph.D.
Assistant Professor, Electro-Optics
Committee member

John Detrio, M.S.
Associate Professor, Electro-Optics
Committee member

Donald L. Moon, Ph.D.
Interim Associate Dean/Director
Graduate Engineering and Research

Joseph Lestingi, D. Eng., P.E.
Dean
School of Engineering

ABSTRACT

MEASUREMENT OF ALTERNATING CURRENT LOSSES IN HIGH-T_c SUPERCONDUCTORS

Name: Kamal Kanti Das
University of Dayton
Advisor: Dr. Binod Kumar

A relatively simple experimental technique was developed to measure alternating current (ac) loss in superconductors. The superconducting specimen was prepared using the solid state reaction method. The effect of electromagnetic radiation on the ac losses was also determined. It was found that the interaction between electromagnetic radiation and the superconductor increases ac loss. The enhancement of ac loss was explained on the basis of the generation of additional charge carriers and their interaction with the lattice. A current-voltage relationship was found by passing an ac current through the sample and measuring the resulting voltage drop. Further, an experiment was performed to investigate the intensity dependence of ac loss. The ac loss was found to increase linearly as the intensity of laser radiation was increased. This resulted from photon absorption and due to an increase of the number of quasi-particles.

ACKNOWLEDGMENTS

The author expresses his deep gratitude to his advisor, Dr. Binod Kumar, for his constant inspiration to bring this work to a conclusion as well as for his patience and expertise. He also thanks his committee members, Dr. Mohammad A Karim, Dr. Gordon R. Little, and Mr. John Detrio, for their helpful suggestions and comments. The author would also like to express his gratefulness to his colleagues, Christina H. Chen, Kapil N. Mirchandani, and Ursula Szmulowicz, for their many and varied contributions and their constructive criticisms. Finally, he sincerely acknowledges the financial support provided by the Aero-Propulsion and Power Directorate of Wright Laboratory, Wright-Patterson Air Force Base, under contract no. F33615-91-C-2156.

TABLE OF CONTENTS

ABSTRACT iii

ACKNOWLEDGMENTS iv

TABLE OF CONTENTS v

LIST OF FIGURES vi

LIST OF TABLES ix

CHAPTER

I. INTRODUCTION 1

II. LITERATURE REVIEW 7

III. STATEMENT OF THE PROBLEM 30

IV. EXPERIMENTS 31

V. RESULTS AND DISCUSSIONS 40

VI. SUMMARY AND CONCLUSIONS 57

VII. RECOMMENDATIONS FOR FUTURE WORK 60

APPENDICES

APPENDIX A 62

REFERENCES 64

LIST OF FIGURES

Figure 2.1	Variation of resistance of metals with temperature	8
Figure 2.2	Loss of resistance of a superconductor at low frequencies.....	9
Figure 2.3	Dependence of the superconducting states on temperature, magnetic field, and current density.....	10
Figure 2.4	Meissner effect in a superconducting sphere cooled in a constant applied field	11
Figure 2.5	(a) Magnetization versus applied magnetic field for a type I bulk superconductor exhibiting a complete Meissner effect (b) Superconducting magnetization curve of a type II superconductor.....	12
Figure 2.6	Schematic representation of flux vortices in a type II superconductor	13
Figure 2.7	The number of superconducting electrons (n_S) increases below T_C	15

LIST OF FIGURES

Figure 2.1	Variation of resistance of metals with temperature	8
Figure 2.2	Loss of resistance of a superconductor at low frequencies.....	9
Figure 2.3	Dependence of the superconducting states on temperature, magnetic field, and current density.....	10
Figure 2.4	Meissner effect in a superconducting sphere cooled in a constant applied field	11
Figure 2.5	(a) Magnetization versus applied magnetic field for a type I bulk superconductor exhibiting a complete Meissner effect (b) Superconducting magnetization curve of a type II superconductor.....	12
Figure 2.6	Schematic representation of flux vortices in a type II superconductor	13
Figure 2.7	The number of superconducting electrons (n_S) increases below T_C	15

Figure 2.8 Reflectivity of polycrystalline $YBa_2Cu_3O_{6.85}$ with T_c = 89K in the normal (solid line) and superconducting (dashed line) states [30] 24

Figure 2.9 (a) Room temperature reflectance of single-crystal $Y_1Ba_2Cu_3O_{7-\delta}$ with T_c= 92K (point) along with a Drude fit (solid line)

(b) Corresponding conductivities calculated from reflectance data via a Kramers-Kronig transformation (dashed line) and from the best Drude fit to reflectance (solid line) [31]..... 26

Figure 4.1 Schematic of the ac loss measurement setup 33

Figure 4.2 Diagram of the Four point probe technique 34

Figure 4.3 Experimental setup to measure the intensity dependence of ac loss 38

Figure 5.1 Impedance of a $Y_1Ba_2Cu_3O_{7-\delta}$:Ag superconductor at 77.2K as a function of frequency..... 42

Figure 5.2 AC loss of $Y_1Ba_2Cu_3O_{7-\delta}$:Ag superconductor 43

Figure 5.3 I-V characteristics of $Y_1Ba_2Cu_3O_{7-\delta}$:Ag superconductor at a frequency of 100 Hz 47

Figure 5.4 AC losses in $Y_1Ba_2Cu_3O_{7-\delta}$:Ag superconductor at a frequency of 100 Hz 48

Figure 5.5 Variation of ac loss of $Y_1Ba_2Cu_3O_{7-\delta}$:Ag superconductor with the power of an Argon-ion laser..... 51

Figure 5.6 Effect of intensity of laser radiation on ac losses of $Y_1Ba_2Cu_3O_{7-\delta}$:Ag superconductor..... 52

Figure 5.7 Quasi-particle generation due to the intensity of laser radiation..... 55

Figure 5.4 AC losses in $Y_1Ba_2Cu_3O_{7-\delta}$:Ag superconductor at a frequency of 100 Hz 48

Figure 5.5 Variation of ac loss of $Y_1Ba_2Cu_3O_{7-\delta}$:Ag superconductor with the power of an Argon-ion laser..... 51

Figure 5.6 Effect of intensity of laser radiation on ac losses of $Y_1Ba_2Cu_3O_{7-\delta}$:Ag superconductor..... 52

Figure 5.7 Quasi-particle generation due to the intensity of laser radiation..... 55

LIST OF TABLES

Table 1	Results of encapsulation and sintering of $Y_1Ba_2Cu_3O_{7-\delta}$:Ag superconductor	31
Table 2	Meissner effect, current density, and T_c of samples E-3 through E-6	32

CHAPTER I
INTRODUCTION

In 1911, H. Kamerlingh Onnes discovered superconductivity in mercury at about 4K. Superconductivity is defined as the property of a material to lose its resistivity by undergoing an electronic phase transformation at low temperatures. The temperature at which a material passes from the normal to the superconducting state is known as the transition or critical temperature (T_c). Superconductors behave like ordinary conductors above T_c but have zero resistance below the T_c.

Superconductivity occurs because a material has less energy in its superconducting state than in its normal state. The theory of superconductivity developed in the 1950's provided an explanation for this lower energy state. Leon Cooper took a significant step in developing the theory of superconductivity in 1956 by calculating what happens when two electrons are added to a metal in the presence of an attractive interaction. He was successful in showing that, in the presence of such an attractive interaction, no matter how weak, two electrons that are added to the Fermi sea will form a bound pair. In 1957, the BCS theory, named after its discoverers, Bardeen, Cooper, and Schreiffer, explained the mechanisms of superconductivity. This theory proposes that electron pairs (Cooper pairs) form due to phonon mediation. As an electron pair moves through the lattice,

it produces a wake. By following in this wake, other paired electrons are able to avoid collisions as they move through the lattice. However, the BCS theory does not adequately explain superconductivity in the present oxide, high-T_c superconductors [1]. In low- T_c superconductors, the mechanism for pair formation is electron-phonon interaction, but other mechanisms involving polarons or excitons may also be responsible for superconductivity in high-T_c materials. Many other theories exist to account for the high transition temperatures of oxide superconductors. While most theories are based on pairing, they differ on the origin of the attractive interaction that gives rise to the pairs and on the strength of the pairs. Observed isotope effects indicate that phonons play a role, but additional mechanisms are necessary to account for high-T_c superconductivity. It has also been suggested that bosons in addition to phonons may be responsible for the attractive interaction between electrons [2].

Before 1986, superconductivity was found only at extremely low temperatures (< 24K). With the discovery of high-T_c superconductivity in copper oxide materials in 1986 [3], applications in various fields, e.g. computer chips and other electronic devices, are emerging. Presently, three types of high-T_c superconductors (HTS) with the T_c > 77K have shown commercial potential. In early 1987, Wu et al. [4] discovered superconductivity in $YBa_2Cu_3O_{7-\delta}$ at a T_c of 92K. In early 1988, a bismuth-based compound, $Bi_2Sr_2Ca_2Cu_3O_x$, was discovered to be a superconductor at a T_c of 110K [5], was followed soon after by the discovery of a Tl-Ba-Ca-Cu-O compound with a T_c of 125K [6]. These oxide superconductors allowed the operating temperature of potential superconducting devices to increase from liquid helium to liquid nitrogen

temperature. This reduces refrigeration costs by several orders of magnitude. In fact, it can lead to a much wider use of superconducting electronic devices in various fields of science, technology, and industry.

There are many applications of superconductors. The major applications can be categorized as small volume, such as electronic and optoelectronic applications, and large volume, which are related to the transmission lines, motors, and generators.

Electronics can be classified into two types: digital and analog. Superconductive electronics can meet the demands of both digital and analog technologies. A large number of applications of superconductors are based on the properties of Josephson junctions [7]. By changing the critical current of a junction, for example, it can be used as a switch. This switching and the hysteretic nature of the I-V characteristic of the junction can be utilized as both logic and memory elements for digital applications. The junctions can also be used to detect electromagnetic radiation over a broad range of frequencies.

Superconductors are found in two distinct types of high power applications: as conductors for magnets or power transmission and as high-power microwave cavities for accelerators or microwave energy storage. Superconducting magnets could provide high fields that are not possible to obtain with conventional conductors. The energy that is stored in a magnetic field is quite considerable. Superconducting magnetic energy storage (SMES) devices can store energy for long periods with virtually no loss [8] and could serve as magnetic batteries, supplying and storing electrical energy

for various purposes. One of the most significant uses of superconducting magnets is in transportation systems featuring magnetically levitated vehicles.

The development of superconducting devices requires an understanding of two major problems - ac resistance or loss and the current carrying capacity. The former is the theme of this thesis.

Electricity, or an electrical current, is the movement of electrons through a material. Ordinary materials resist the flow of electricity to varying extents. Even extremely good conductors such as Cu, Ag, and Au consume some amount of energy during the flow of current. Because some energy is used up to overcome the resistance it requires a voltage to sustain a current . The resistance arises when the lattice scatters electrons, causing them to lose their motion in a conductor, which results in the heating of the conductor (Joule heating). On the other hand, no energy is needed to sustain current flow in a superconductor. Its electrical resistance is zero below the T_c. This means that the voltage drop across the superconductor is zero when a current is passed through it. Ideally, no power should be dissipated as a result of the passage of current. Yet, this zero resistance property of superconductors is true only for a dc current. If the current changes, an electric field will develop and some power will be dissipated. This dissipative power per specimen cross-sectional area is termed ac loss. This resistance or ac loss is frequency and temperature dependent. In fact, the higher the frequency of the ac current, the higher the resistance of the superconductor. At low frequencies, losses are primarily due to flux creep (see Appendix A for details), hysteresis, and related magnetic phenomena. At microwave frequencies, surface resistance increases by the square of frequency. As

frequency approaches the optical range, the superconductor gradually loses its superconducting properties.

The current carrying capacity of most HTS films is around 10^4 A/cm^2. For applications such as power transmission lines, current limiters, etc., the required critical current density at 77K should be of an order of 10^5-10^6 A/cm^2. Amongst the three high-T_c copper oxide superconductors, the $YBa_2Cu_3O_{7-\delta}$ (also called 123) superconductor appears to be the most promising for immediate applications. This compound exhibits less flux creep effect than the other two material systems, which implies that it is more stable with respect to supercurrent under a magnetic field. The theoretical upper value of the critical current density (J_c) is 2.3×10^8 A/cm^2 at 0°K, based on the calculated value from the Ginzburg-Landau equation [9]. After applying a magnetic field of 1 tesla, this value decreases to 2.7×10^7 A/cm^2 at the liquid nitrogen temperature. For practical applications, a J_c of about 10^5 A/cm^2 at 77K and a field of 5 tesla [10] is required. The techniques for shaping superconducting materials in useful forms, such as wires, tapes, or films, need to be developed and refined so as to improve the critical current density.

The purpose of this thesis is to develop an experimental technique to measure ac loss in superconductors and to assess the effect of the electro-magnetic radiation associated with the measurement of ac loss.

The thesis consists of seven chapters. Chapter II provides a background review of the various properties of superconductors. This includes the basic phenomenon of superconductivity, the relevant properties of ac the loss mechanisms, and the optical and optoelectronic properties of

superconductors. Chapter III states the problem of this thesis work. The development of the ac loss measurement technique is presented in chapter IV. This chapter also includes a discussion of superconducting specimen preparation technique and the effect of electromagnetic radiation on ac loss. Chapter V explains the results of ac loss measurement as well as the effect of electromagnetic radiation and the intensity dependence of the ac loss of superconductors. Next, chapter VI presents a discussion pertaining to the works carried out in this thesis. Finally, chapter VII suggests the directions for future studies.

CHAPTER II
LITERATURE REVIEW

This chapter reviews previous works on the various properties relevant to ac loss and the electromagnetic effects of superconductors. It begins with a discussion of the basic phenomenon of superconductivity. Subsequent topics include the two-fluid model, electrodynamic properties, ac loss mechanisms, surface resistance, and optical and optoelectronic properties. All these topics complement this thesis' focus on the origin and measurement of ac losses.

2.1 Basic Phenomenon of Superconductivity

(A) Normal State

In general the electrical resistivity of metals and alloys decreases when they are cooled below a certain temperature. The current in a metal or alloy conductor is carried by "conduction electrons" or "free electrons" which move freely through the material. Electrons behave like a wave; an electron traveling through a metal can be represented as a plane wave progressing in the direction of the wave. Usually, a metal has a crystalline structure with its atoms lying on a regular repetitive lattice. It is a property of a plane wave that it can pass through a perfectly periodic structure without being scattered in many directions. Thus, an electron is able to pass through a perfect crystal without any loss of momentum in

its original direction [11]. This implies that if, in a perfect crystal, a current is flowing, the current will experience no resistance. However, any disarray in the periodicity of the crystal will scatter the electron wave and introduce some resistance. There are two effects which can disorder the perfect periodicity of a crystal lattice and so introduce resistance. At temperatures above or even at absolute zero, atoms vibrate and are displaced by various degrees from their equilibrium positions. Also, randomly-distributed foreign or other defects can interrupt perfect periodicity. Both the thermal vibrations and any impurities or imperfections scatter the moving conduction electrons and give rise to electrical resistance.

However, as the temperature is lowered, the thermal vibrations of the atoms decrease and the conduction electrons are less scattered. The decrease of resistance is linear until the temperature is equal to about one-third of the characteristic Debye temperature (θ_D) of the material. However, as the temeperature falls below the Debye temperature, the resistance decreases less rapidly, as is shown in Figure 2.1. For a pure metal, where electron motion is impeded only by the thermal vibrations of the lattice, resistivity should approach zero as the temperature is reduced to 0°K. This zero resistance, which a completely pure specimen would acquire if it could be cooled to absolute zero, is not a phenomenon of superconductivity. Any real specimen of conductor cannot be completely pure but will contain some defects. Therefore, the electrons, in addition to being scattered by the thermal vibrations of the lattice atoms, are also scattered by impurities; this impurity scattering is more or less independent of temperature near the absolute zero. As a result, there is a certain "residual resistivity" (ρ_0) which remains even at the lowest temperatures.

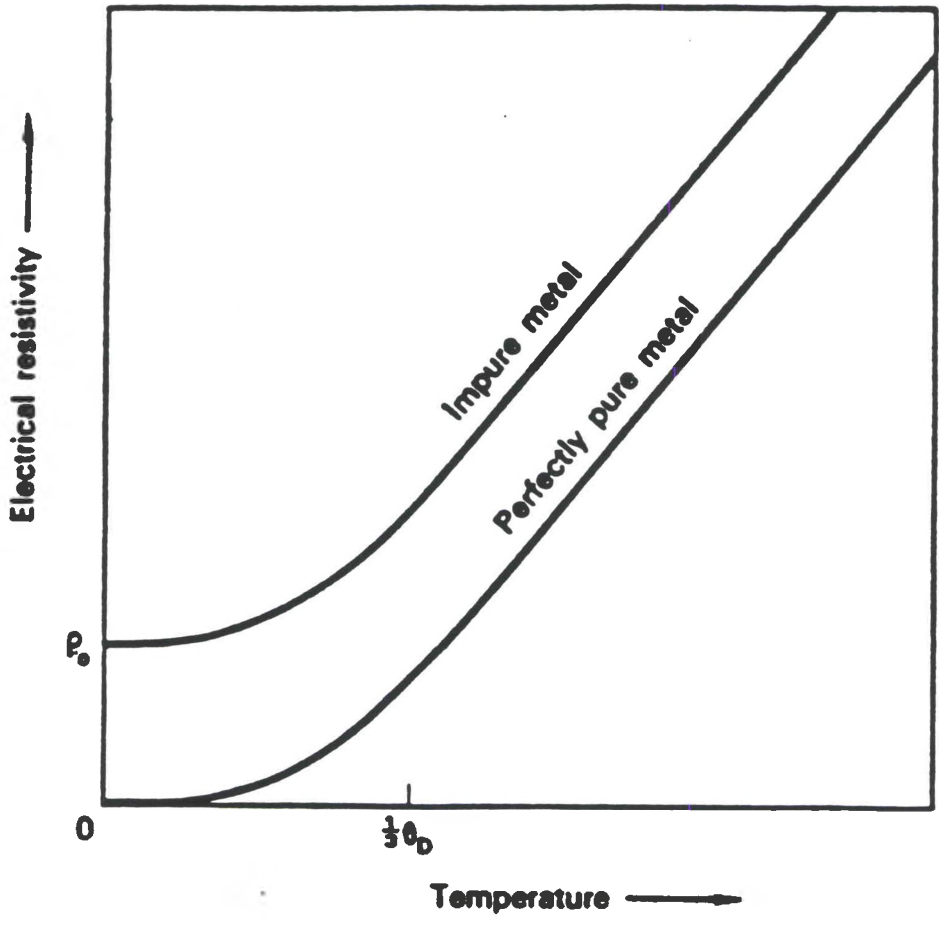

Figure 2.1 Variation of resistance of metals with temperature

(B) Superconducting State

Certain elements and alloys show very remarkable behavior in that, if they are cooled, their electrical resistance decreases in the usual way but, upon reaching

a temperature well above absolute zero, they suddenly lose all trace of electrical resistance, as shown in Figure 2.2. The materials then pass into the

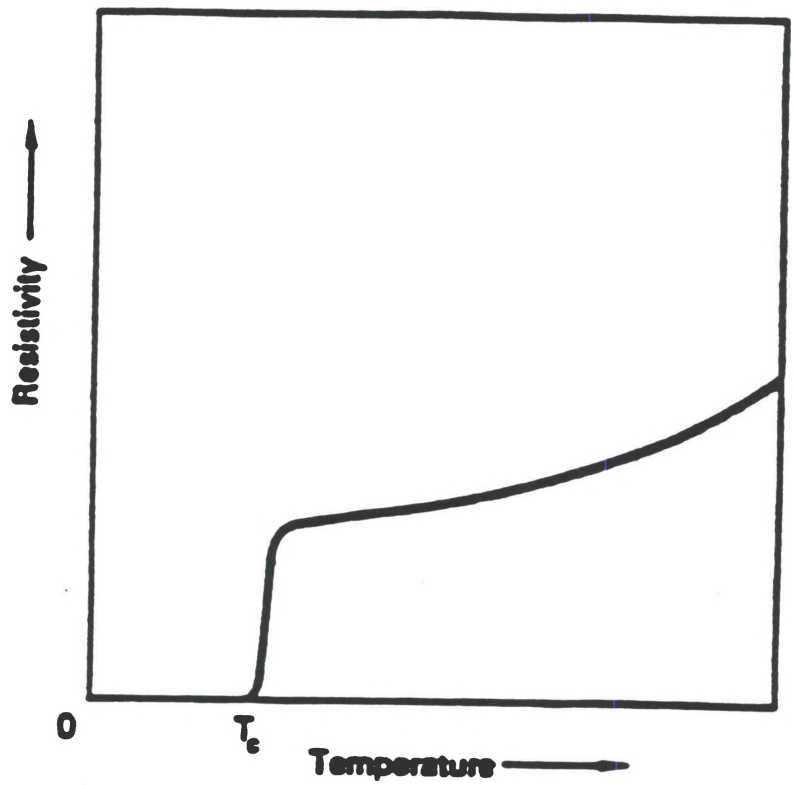

Figure 2.2 Loss of resistance of a superconductor at low temperatures.

superconducting state. The transformation to the superconducting state may occur even if the material is impure. This superconducting state is present only in a particular range of temperature, magnetic field strength, and current density. The condition for the superconducting state to exist in a material is that some combination of temperature, magnetic field strength, and current density be less

than certain critical values; as shown in Figure 2.3. The critical values of the field strength and temperature are experimentally found to follow the equation:

$$H_c = H_0[1-(T/T_c)^2] \qquad (2.1)$$

where H_c is the critical field strength at temperature T, H_0 is the maximum critical field strength at absolute zero, and T_c is the critical temperature.

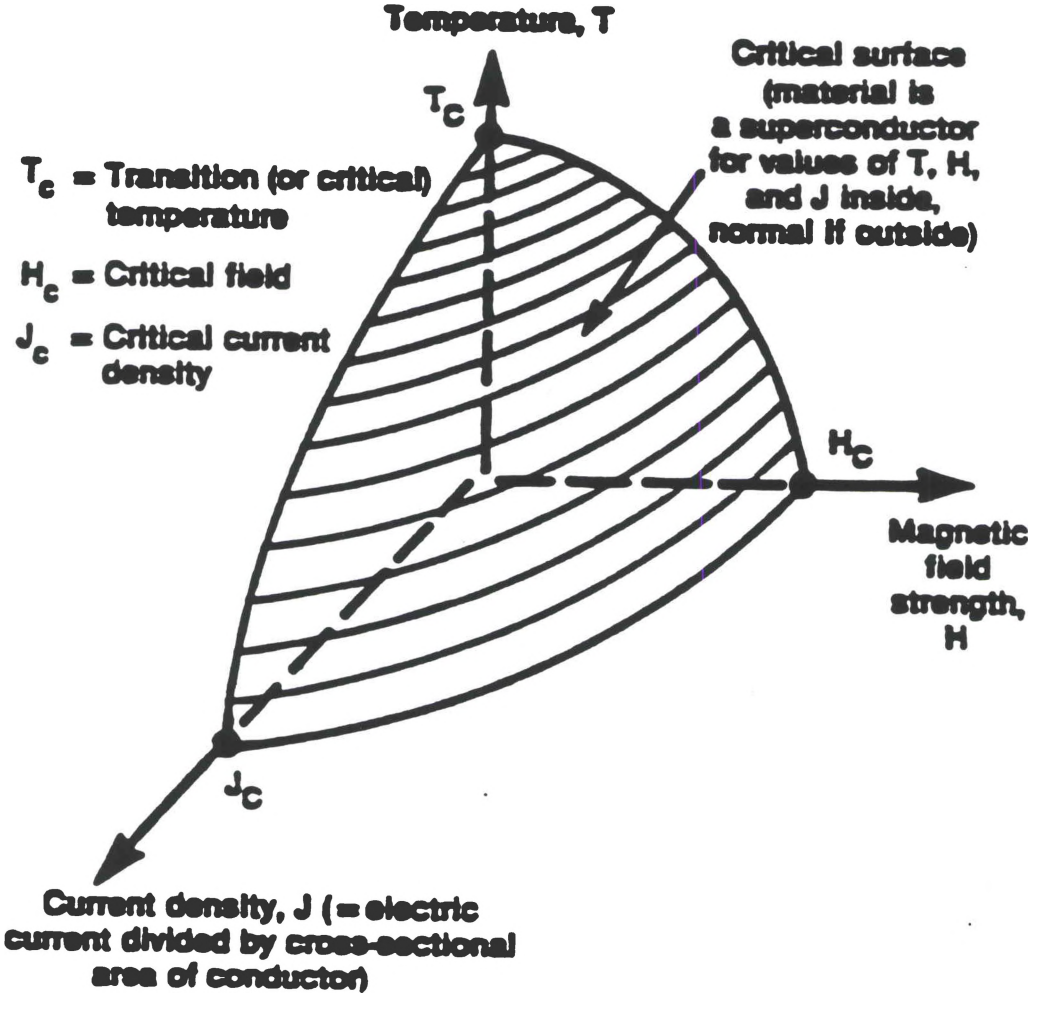

Figure 2.3 Dependence of the superconducting states on temperature, magnetic field, and current density.

(C) Meissner Effect

Meissner and Ochsenfeld [12] found that, if a superconductor in a magnetic field is cooled to a temperature below the transition temperature, then, at the transition, the lines of induction B are pushed out as in Figure 2.4. This phenomenon is the Meissner effect. Thus a bulk superconductor in an external magnetic field, H, shows that as if specimen has $B = H + 4\pi M = 0$ or $\chi = -1/4\pi$, where M is magnetization and χ is magnetic susceptibility. That is, a superconductor exhibits diamagnetism.

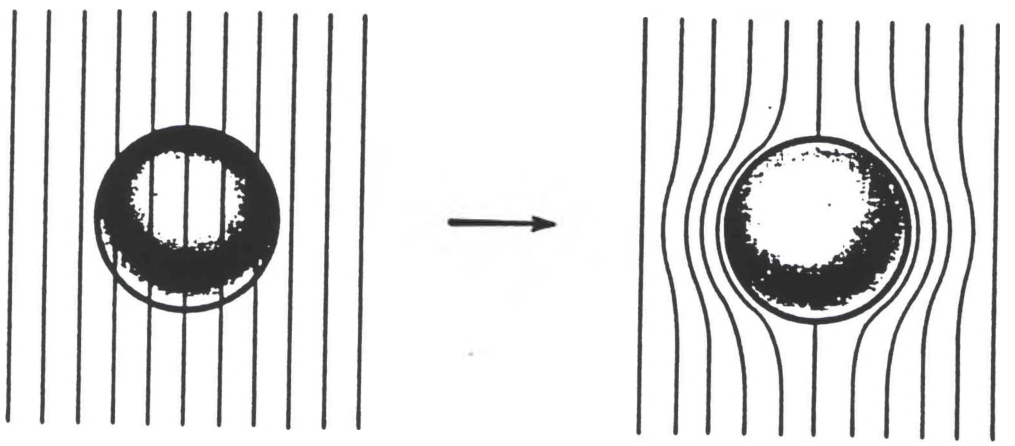

Figure 2.4 Meissner effect in a superconducting sphere cooled in a constant applied magnetic field.

(D) Type I and Type II Superconductors

Superconductors are classified into two types according to their response to an applied magnetic field, as shown in Figure 2.5. Type I superconductors, which include most metal superconductors, exclude magnetic flux until a maximum field (H_c) is exceeded, at which point the material loses its superconductivity.

In general, type I superconductors are not technologically important because their H_c is very low (0.01 to 0.1 tesla).

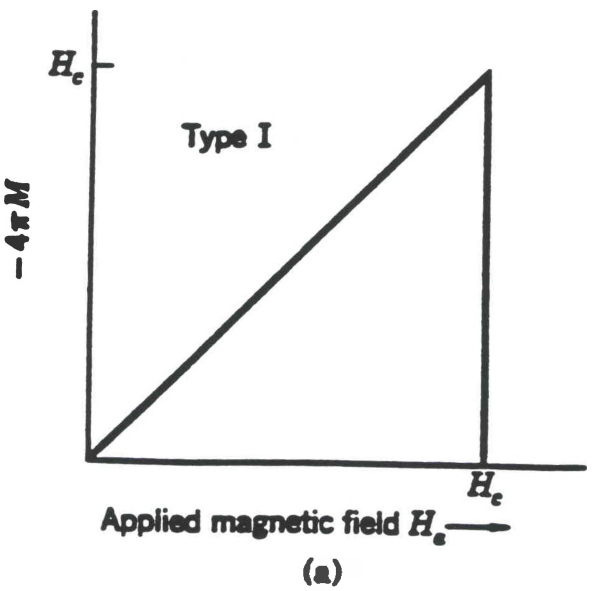

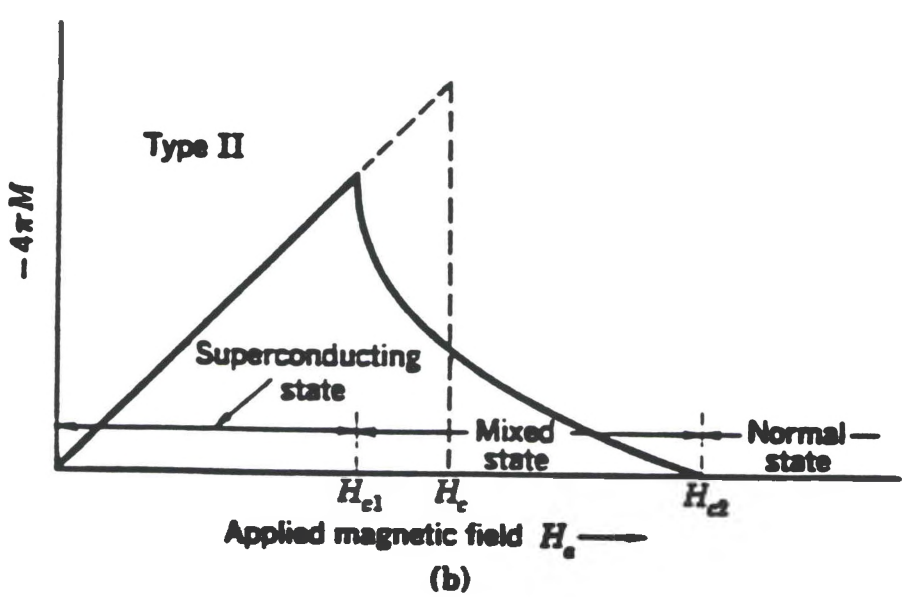

Figure 2.5 (a) Magnetization versus applied magnetic field for a type I bulk superconductor exhibiting a complete Meissner effect

(b) Magnetization curve of a type II superconductor.

Virtually all superconductors of technological importance are type II, which has two critical fields, H_{c1} and H_{c2}. They behave like type I materials at low magnetic fields (below H_{c1}). At fields above H_{c2}, the material is driven into its normal state. For fields between H_{c1} and H_{c2}, the magnetic flux is partially excluded and the magnetic field penetrates the superconductor, forming a lattice of vortices or supercurrent "whirlpools," as in Figure 2.6.

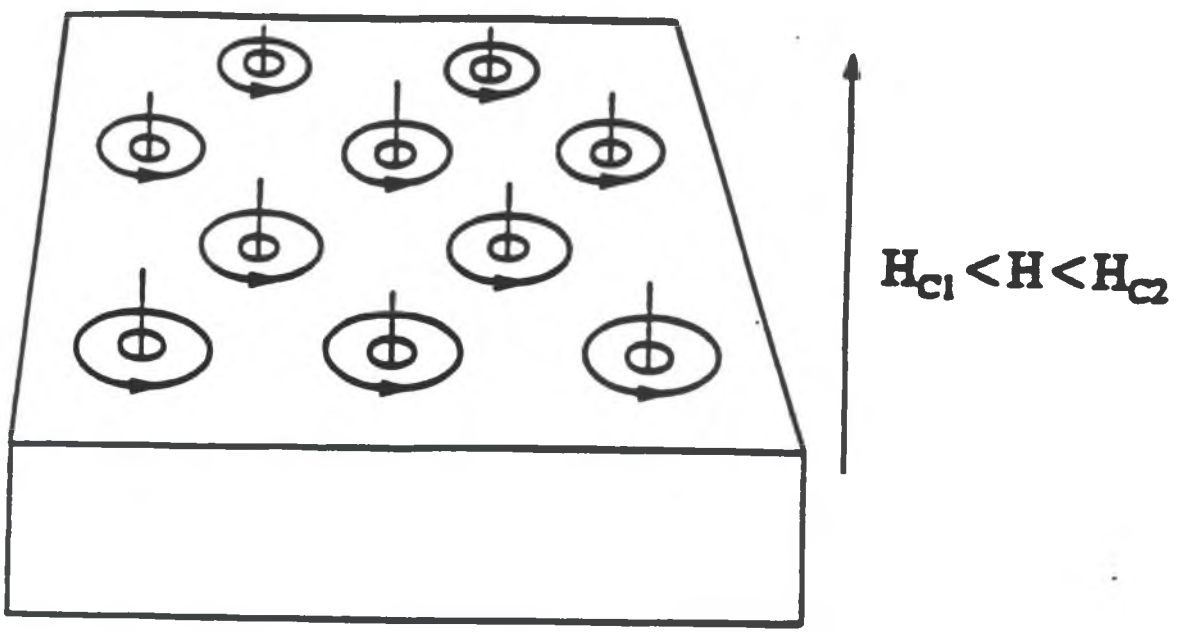

Figure 2.6 Schematic representation of flux vortices in a type II superconductor.

These vortices repel one another and arrange themeselves in a regular array so as to be as far from one another as possible. As the magnetic field is increased toward H_{c2}, more vortices are formed, and lattice spacing is decreased until, at H_{c2}, superconductivity disappears.

In type II materials, defects play an important role in the flow of current. At field strengths above H_{c1}, magnetic flux penetrates the superconductor in the form of flux tubes or filaments. In defect-free materials these filaments are able to move easily into the superconductor to take up their equilibrium configuration. Removing the field reverses the process, and the filaments move out. However, the defects in the material are able to "pin" the flux and prevent or restrict their movement. The presence of defects which pin the flux filaments is important because they increase the capacity of the superconductor to carry current without dissipating power [13]. Defects can be introduced and controlled by standard metallurgical processes such as heat-treatment, ageing and sintering.

2.2 Two-Fluid Model of Superconductivity

The two-fluid model describes the superconducting phenomenon based on the coexistance of superconducting electrons and normal electrons within a superconductor. This model postulates that not all conduction electrons participate in superconducting behavior. As a superconductor is cooled below T_c, normal electrons condense into superconducting pairs. These pairs consist of electrons with opposite spins but equal momenta, this, net momentum and spin of the pair are zero [14]. As the temperature approaches 0K, more normal electrons are converted into paired electrons. Therefore, the number of unpaired electrons diminishes as the temperature decreases. The ratio of normal (n_n) and superconducting (n_s) electrons falls as the temperature decreases below T_c; normal electrons disappear at $T = 0$ while superconducting electrons vanish at $T \geq T_c$, as shown in Figure 2.7. If the density of superconducting electrons is n_0 at 0K, the density of n_s at temperatures below T_c is:

$$n_s = n_o\{1-t^4\} \qquad (2.2)$$

where t is the reduced temperature defined as $t = \frac{T}{T_c}$ [15].

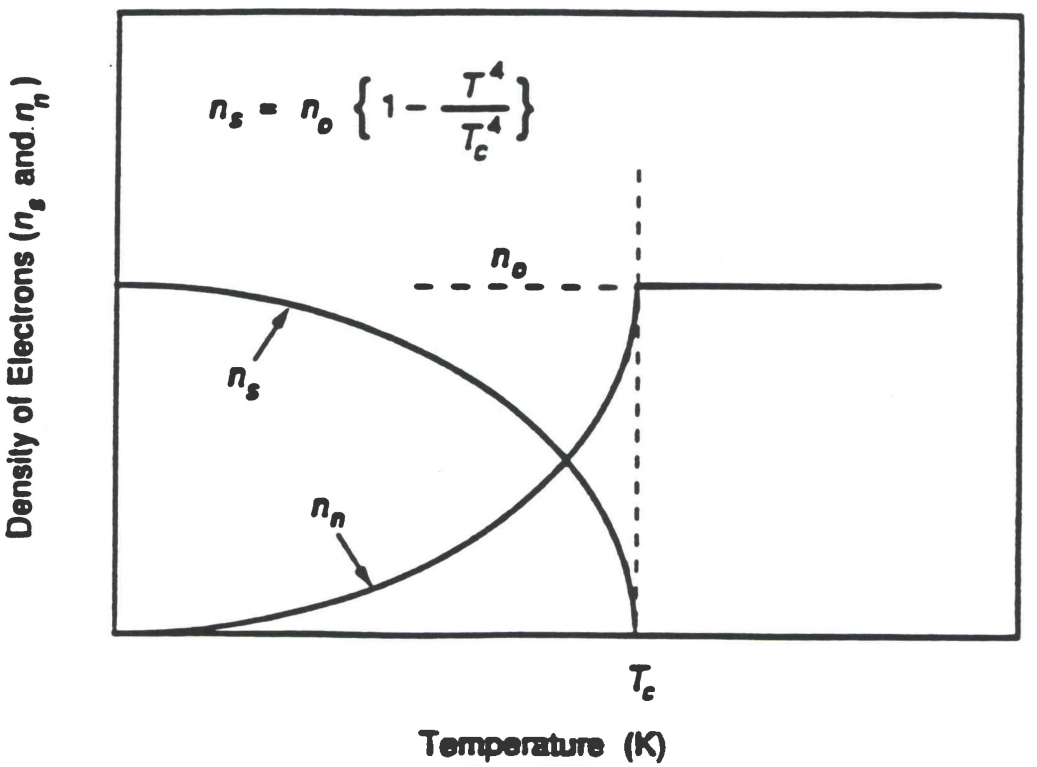

Figure 2.7 The number of superconducting electrons (n_S) increases below T_C.

The total current flowing in the superconductor, according to the two-fluid model, is the sum of the normal and superconducting components:

$$\bar{J} = \bar{J}_s + \bar{J}_n \qquad (2.3)$$

where $\bar{J}_s$ is superconducting current density and $\bar{J}_n$ is normal current density. The normal electron current obeys Ohm's law, that is,

$$\sigma = \frac{\bar{E}}{\bar{J}_n} \tag{2.4}$$

where $\bar{E}$ is the electric field and σ is the temperature dependent electrical conductivity.

2.3 Electrodynamic Properties of Superconductors

If one considers an electron with mass m and charge e in an applied electric field, $\bar{E}$, the force is given by

$$\bar{F} = m\frac{d\bar{v}}{dt} = e\bar{E}. \tag{2.5}$$

Current density $\bar{J}$ is simply $ne\bar{v}$, where n is the density of electrons and $\bar{v}$ is the velocity , so that

$$\frac{d\bar{v}}{dt} = \frac{1}{ne}\left(\frac{d\bar{J}}{dt}\right) = \frac{e}{m}\bar{E} \tag{2.6}$$

and

$$\frac{m}{ne}\frac{d\bar{J}}{dt} = e\bar{E}. \tag{2.7}$$

Thus,

$$\frac{d\bar{J}}{dt} = \left(\frac{ne^2}{m}\right)\bar{E} = \left(\frac{1}{\Lambda}\right)\bar{E} \tag{2.8}$$

where $\Lambda = \frac{m}{ne^2}$.

According to this equation, constant currents in superconductors are possible when $\bar{E} = 0$. By taking the curl of both sides of equation (2.8) and using Maxwell's equations, one obtains

$$\bar{\nabla} \times \left(\Lambda\frac{d\bar{J}}{dt}\right) = -\frac{d\bar{H}}{dt}. \tag{2.9}$$

Inside a superconductor, displacement current is negligilble in comparison to $\bar{J}$, so the above equation can be written as

$$\bar{\nabla} \times (\Lambda \frac{d\bar{J}}{dt}) = \Lambda(\bar{\nabla} \times \bar{\nabla} \times \dot{\bar{H}}) = -\frac{d\bar{H}}{dt} \qquad (2.10)$$

which reduces to

$$\Lambda \nabla^2 \dot{H} = \dot{H} \qquad (2.11)$$

After integrating with respect to time, it takes the form

$$\Lambda \nabla^2 (\bar{H} - \bar{H}_0) = \bar{H} - \bar{H}_0 \qquad (2.12)$$

where H_0 denotes the field at time t = 0.

Equation (2.12) is a direct consequence of Maxwell's equations and the acceleration equation (2.5). The results admit the particular solution $\bar{H} = \bar{H}_0$, where $\bar{H}_0$ is an arbitrary field existing at t = 0, but contradicts the Meissner effect because there is a residual field inside the superconductor.

Thus, F. and H. London suggested [16] the second London equation of the form

$$\bar{\nabla} \times \bar{J}_s = -\frac{\bar{H}}{\Lambda} \qquad (2.13)$$

in which Λ is defined as:

$$\Lambda = \frac{m^*}{n_s e^{*2}} = 4\pi\lambda^2 \qquad (2.14)$$

where m^* is the effective mass [17]of the superconducting charge carrier, n_s is the superconducting electron density, e is the electron charge, and λ is a characteristic penetration depth. Even after considering the paired charges, $m^* = 2m$, $e^* = 2e$, and $n = \frac{n_s}{2}$, the value of Λ does not change. Thus, the London equation may be rewritten as

$$\bar{H} = -4\pi\lambda^2 \nabla \times \bar{J}_s \qquad (2.15)$$

and

$$\bar{E} = 4\pi\lambda^2 \frac{\partial \bar{J}_s}{\partial t}. \qquad (2.16)$$

These two equations, which together describe the electrodynamics of the supercurrent, are known as the London equations. Equation (2.16) thus effectively replaces Ohm's law for superconductors describing the conductive property of a superconductor, and equation (2.15) describes diamagnetism. If current density $\bar{J}_s$ does not change with time, the field $\bar{E}$ is required to be zero. Since static supercurrents can flow with a zero electric field, the expression properly describes the superconducting state.

2.4 Consequences of London's Equations

Consider a superconductor that has dimensions much larger than the penetration depth, λ, the depth at which the current persists, and that operates at a temperature of $T \langle\langle T_c$., In this state, a surface alternating electric field, $\bar{E}_s$, at radial frequency ω penetrates the conductor but is attenuated exponentially by a characteristic depth of $\frac{1}{k}$:

$$\bar{E} = \bar{E}_s e^{-kz} \qquad (2.17)$$

The parallel $\bar{H}$ field and surface current also decay likewise.

$$\bar{H} = \bar{H}_s e^{-kz} \qquad (2.18)$$

and

$$\bar{J} = \bar{J}_s e^{-kz} \qquad (2.19)$$

Parameter k is a function of penetration depth (λ) and skin depth (δ):

$$k = \frac{1}{\lambda\sqrt{2}}\left\{\sqrt{n+1} + j\sqrt{n-1}\right\} \qquad (2.20)$$

where $n = \sqrt{1 - \frac{4\lambda^4}{\delta^4}}$.

Skin depth is a measure of the exponential penetration of plane electromagnetic waves into a conductor. Equation (2.20) reduces to [18]

$$k = \frac{1}{\lambda}\sqrt{1 + j2(\frac{\lambda}{\delta})^2} \qquad (2.21)$$

The above expression can be rewritten using δ_L in the following form

$$k = \frac{1}{\lambda}\sqrt{1 + j(\frac{\lambda}{\delta_L})^2} \qquad (2.22)$$

where $\delta_L = \frac{\delta}{\sqrt{2}}$. Parameter δ_L is not skin depth but a related "small length" defined by London [16].

The effects of skin depth limit the flow of electricity to the surface of a conductor at a high frequencies. Parameter λ performs a similar function to δ over a wide range of frequencies. The effects of λ dominates at most frequencies of interest; that is, λ determines the penetration depth of the electromagnetic fields into the material. For a specific superconductor, there is a relatively high frequency where skin depth δ and London penetration depth λ will have the same value. As the frequency increases above that level, the skin depth will continue to decrease while λ does not change. Thus, δ becomes the predominant factor in determining electromagnetic penetration and surface resistivity. The relevant relationship developed by London is

$$\left|\frac{J_n}{J_s}\right| = \left(\frac{\lambda}{\delta_L}\right)^2 = \sigma\Lambda\omega \qquad (2.22)$$

where σ is conductivity and $\Lambda = m/ne^2$ has a typical value on the order of 10^{-31} s^2.

Thus, at frequencies of general interest ($\omega < 1/\sigma\Lambda$), the penetration of surface currents is controlled by λ, which is much smaller than δ_L. For high frequencies ($\omega > 1/\sigma\Lambda$), skin effects gradually begin to dominate over λ. For much higher (optical) frequencies, the superconductor behaves essentially as a normal conductor.

2.5 AC Loss Mechanisms

An understanding of ac loss in high-T_c superconductors is important in the design and development of superconducting devices. Superconductors under steady dc conditions can be operated without dissipating any power, but there will be losses if the current is continually changing. One way to explain these losses is that the ac creates an alternating field at the surface of the superconductor, so that with high peak currents the material is constantly being driven around its cycle of magnetization. The magnetization curves of the superconductors exhibit hysteresis, so the energy losses that occur under ac conditions are hysteresis losses.

Many experiments have been performed to measure these losses, but there has been no detailed explanation of the mechanism involved. Buchhold [19] deduced that the losses may be due to field enhancement and the consequent flux penetration at surface irregularities. Buchhold and Rhodenizer [20] attempted to solve the problem by assuming a field dependence of the London penetration depth. In addition to the intrinsic loss due to flux penetration at peaks in the surface, flux trapped in a direction perpendicular to the surface can enhance the ac loss in superconductors. However, calorimetric loss measurements by Buchhold and Molenda [21] and Rocher and Septfonds [22]; and electrical measurements by

Male [23] show that this is an effect independent of the flux penetration loss. AC loss experiments with the external magnetic field parallel to the surface show that the loss starts from very small fields [22]. It can be assumed that flux penetration begins with a zero field and that there is no discontinuity in the flux density at the highest peaks in the surface. Flux can enter the peaks at a low field but cannot enter the bulk until the external field exceeds the lower critical field, H_{c_1}. Thus, it is expected that no hysteresis losses should arise if the peak surface field produced by the current remains less than this critical field.

The next major problem is to calculate the amount by which the magnetic field is enhanced at peaks arising from surface irregularities. This requires a solution using the Laplace equation with rather difficult boundary conditions[24]. Experiments and calculations on electrical breakdowns show that an electric field is enhanced by a factor of 10-100 on very smooth surfaces [25-28]. This value may differ depending on the type of surface. In electrical breakdown experiments, the electric field is applied perpendicular to the surface, but a magnetic field parallel to the surface should be enhanced by a similar amount. The electric field must be kept below the breakdown value, but, for all practical purposes, the external magnetic field will be much greater than the lower critical field, H_{c_1}. Kulik [29] has shown that an ellipsoid with demagnetizing coefficient n enters the mixed state at field $(1-n)H_{c_1}$. A demagnetizing coefficient cannot be assigned to a non-ellipsoidal body, in which case only part of the superconductor goes into the mixed state while the rest remains in the Meissner state. In particular, fluxons, the quanta of magnetic flux, can be expected to enter peaks in the surface of an essentially flat superconductor at very low fields. As stated earlier, it cannot enter the bulk until the external field exceeds H_{c_1}. If the field produced by the current

exceeds H_{c_1}, hysteresis losses appear which at low frequencies are expected to increase linearly with frequency.

2.6 Frequency Dependence of Surface Resistance

Helmut Piel [30] suggested the following approach to account for the frequency dependence of superconductor surface resistance. Consider the alternating magnetic field, H_S, which is parallel to the surface of a superconductor. According to the Faraday induction law, the magnitude of induced surface field E_S is proportional to the product of ω and B_S:

$$E \propto \omega B_S \tag{2.23}$$

The electric field generates losses due to the normal electrons that still exist above $0^{\circ}K$. The normal conductance associated with these unpaired electrons is represented here by σ_e and is given by

$$\sigma_e = \frac{n_e e^2 l}{2mv_0} \tag{2.24}$$

where n_e = density of normal electrons,

l = mean free path, and

v_0 = mean velocity.

The surface power density (P_S) over an area A for an incremental volume , dV, in terms of E_S can be expressed as:

$$P_s = \frac{\sigma_s E_s^2}{2} (dV) \propto \frac{\sigma_e E_s^2}{2} (A\, \lambda). \tag{2.25}$$

The factor "2" is used in the denominator because E and H represent peak values of a sinusoidal field. Since E_S is proportional to ωB_S (or ωH_S), equ. (2.25) can be written as

$$\frac{P_s}{A} \propto \frac{\sigma_e(\omega H_s)^2}{2}\lambda. \qquad (2.26)$$

Also, P_S can be expressed in terms of surface resistance and surface field H_S by

$$\frac{P_s}{A} = \frac{R_s H_s^2}{2}. \qquad (2.27)$$

Thus, one can obtain

$$R_s \propto \sigma_e \omega^2. \qquad (2.28)$$

In general, R_S is proportional to $\omega^{\frac{1}{2}}$ for normal conduction and to $\omega^{\frac{1}{3}}$ or $\omega^{\frac{2}{3}}$ for cryogenic cavities at sufficiently high frequencies. Superconductors have a surface resistance that varies as ω^2, except for the residual component for $T \langle\langle T_c$.

2.7 Optical Properties of High-T_c Superconductors

High-T_c superconductors exhibit anisotropic behavior in the optical response as well as in the transport of electric current. The properties of these materials are not widely understood because of the complications involving optical anisotropy, materials preparation, sensitivities to stoichiometry, and impurity concentrations. The difficulties of preparing sufficiently large and uniform high-quality single-crystals make spectroscopy work particularly challenging. Infrared (IR) spectroscopy of superconductors has received considerable attention because the optical response in this spectral region is dominated by the free carriers [31]. The situation in the IR can be improved with single crystals of sufficient size and homogeneity for spectroscopic measurements. The IR optical responses of the basal plane and in the perpendicular direction have been accurately determined by reflectometry for $Y_1Ba_2Cu_3O_{7-\delta}$ [32-34]. Experimental consistency is achieved with single-crystal samples, but interpretations of these data remain controversial.

The situation in the visible-near-ultraviolet (V-NUV) range is better, partly because of the greatly reduced optical anisotropy and the availability of alternative measurement techniques. Optical techniques such as spectroellipsometry are available to obtain accurate dielectric function data. The dielectric function can be accurately simulated by the Drude model [32,33].

Mattis and Bardeen have shown that, when a material is superconducting, its optical response is expected to appear at energy $\omega_\Delta = 2\Delta$, where 2Δ is the superconducting energy gap [35]. The BCS value of 2Δ is 3.53 $K_B T_c$, where K_B is Boltzmann's constant. But strong-coupling theories predict values as high as 11.5 $K_B T_c$ for the 2Δ [36]. Other theories predict that superconductivity in these materials is gapless [37]. Consequently, the optical response corresponding to the superconducting gap should be found roughly between 100 and 320 cm^{-1} for $La_{1.85}Sr_{0.15}CuO_{4-\delta}$ with T_c = 40K, 220 and 735 cm^{-1} for $YBa_2Cu_3O_{7-\delta}$ with T_c = 92K, and 300 and 1000 cm^{-1} for $Tl_2Sr_2Ca_2Cu_3O_{10}$ with T_c = 125K. Thus, a fairly wide spectral range is involved.

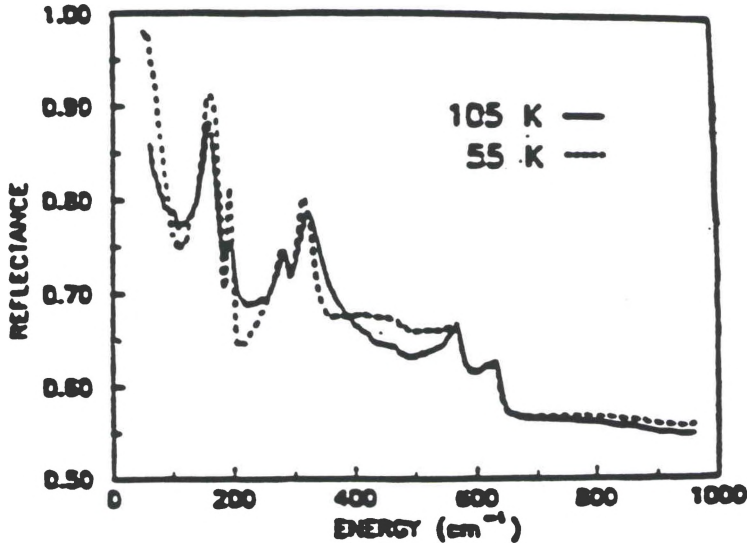

Figure 2.8 Reflection of polycrystalline $YBa_2Cu_3O_{6.85}$ with T_c= 89 K in the normal (solid line) and superconducting (dashed line) states.

All presently available data that can estimate the superconducting energy gap are in the form of normal incidence reflectance. Data for polycrystalline [38] and single-crystal [32] $YBa_2Cu_3O_{7-\delta}$ samples are shown in Figures 2.8 and 2.9, respectively. The Drude model is the usual framework to analyze the data, as in Figure 2.9. The fundamental response of the material is described by the dielectric function, $\varepsilon(\omega) = \varepsilon_1 + i\varepsilon_2$.

The optical response of Figure 2.9 can be described approximately in terms of the general expression for the dielectric response of a damped oscillator. The detailed mathematical expressions that describe the dielectric response of the superconducting state were derived by Mathis and Bardeen [35]. In fact, reflectance does not provide direct information on the excitations that give rise to the optical response. In order to get direct information about conductivity, the reflectance data need to be converted to the dielectric constant, ε, by means of the Kramers-Kronig transform.

2.8 Optoelectronic Properties of Superconductors

Currently, optoelectronics is a developing area of engineering and technology where high-temperature superconductors (HTS) may have various types of applications. The HTS materials are perovskites whose crystalline structure is very similar to several optoelectronic materials. This characteristic can be exploited to promote the epitaxial growth of HTS films on electro-optic substrates. Perovskites are abundant minerals and, in their ideal form, are cubic with a highly symmetrical arrangement of atoms. However, in reality, perovskites with lower symmetry structures (e.g., tetragonal, triangular, or orthorhombic) are very common. Interestingly, these deviations from the ideal cubic structure of

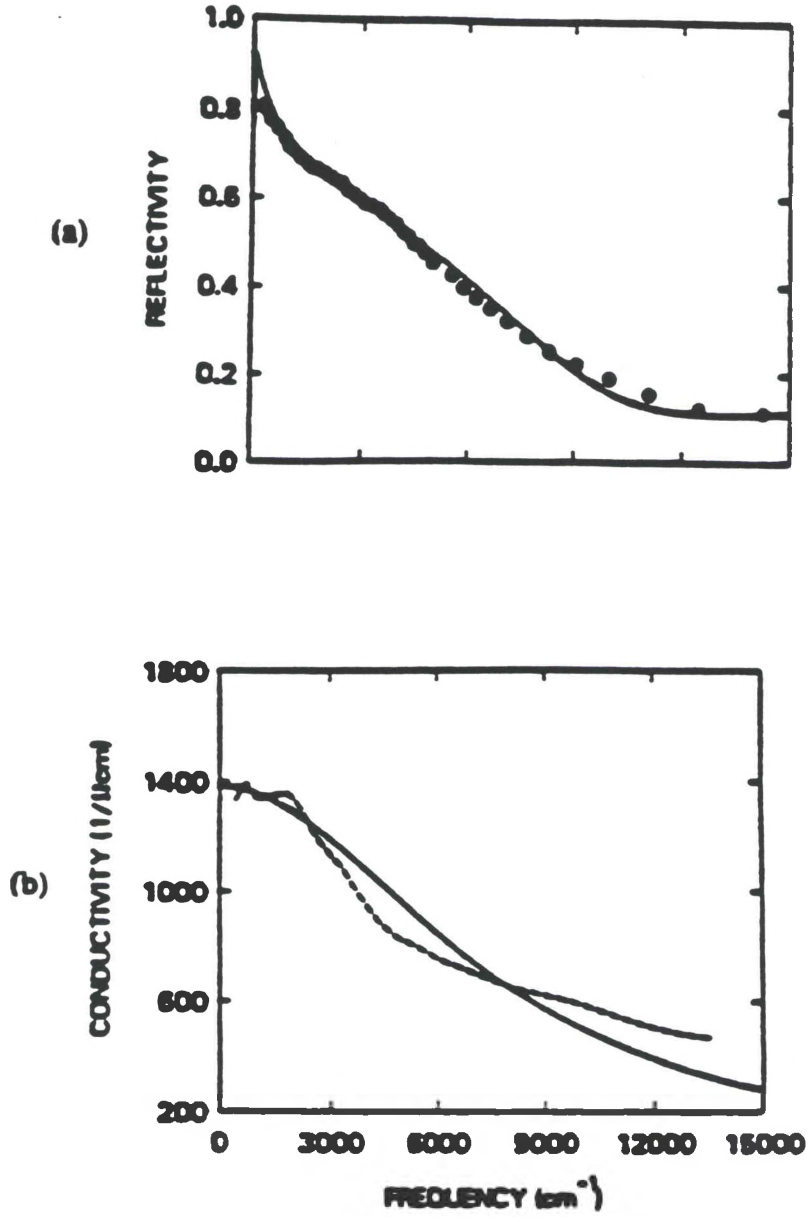

Figure 2.9 (a) Room temperature reflectance of single crystal $YBa_2Cu_3O_{7-\delta}$ with T_c = 92K (point), along with a Drude fit (solid line).

(b) Corresponding conductivities calculated from reflectance data via a Kramers-Kronig transformation (dashed line) and from the best Drude fit to reflectance (solid line).

perovskites lead to an array of different electrical and/or optical properties [39]. The electrical and optical properties of HTS crystals are very sensitive to small variations of their crystallographic structure and of their atomic composition in the elementary cell.

An ideal bulk superconductor below T_c is a perfect reflector of electromagnetic radiation at low-to-moderate frequencies. If the energy associated with a particular photon frequency ($h\nu$) is greater than the superconductor's energy gap, the material will absorb electromagnetic radiation.

Superconducting films have been proposed for the detection of microwave and IR radiation. Superconducting photon detectors require less power, respond faster, and a have larger bandwidth (extending to long-wave IR) than conventional detectors. The sensitivity of conventional superconductor detectors extends to wavelengths of several hundred μm; however, typical semiconductor detectors can be used at a maximum wavelength of 20 μm.

Detection mechanisms are classified as thermal (i.e., bolometric) or nonthermal. In the thermal case, the temperature of the sensor is increased by the absorption of radiation. The nonthermal mechanism depends on the creation of quasi-particle pairs, which is induced by the incident photon. In this case, Rose et al. [40] have shown that the mechanisms depend on the non-linearity of the voltage-current characteristic of the film.

Optoelectronic devices require that the films be fabricated on compatible electro-optical materials. Generally, the high-speed analog application (including optoelectronics) of HTS films calls for high quality dielectric substrates. Substrate materials can be selected on the basis of the crystalline structure quality of the

deposited film. A. Hohler et al. [41] and S.G. Lee et al. [42] have succeeded in fabricating good, nearly epitaxial films on $LiNbO_3$. This may stimulate the progress in developing hybrid HTS/$LiNbO_3$ optoelectronic devices.

Nonlinear optical materials are esssential for optoelectronic applications. Below the transition temperature, HTS materials are not likely to display useful nonlinear optical properties since the electromagnetic field cannot penetrate the volume of the superconductor. However, several different groups [43-47] have shown that, above the critical temperature and/or in the oxygen-depleted HTS phase, 123 superconductors show an interesting photovoltaic effect. This effect implies that HTS films could have electro-optic properties.

CHAPTER III

STATEMENT OF THE PROBLEM

The primary objective of this study was to develop an experimental technique to measure ac loss in high-T_c superconductors. In addition, a secondery objective was to investigate the effect of electromagnetic radiation on ac losses.

The specific tasks of this investigation were the following:

(i) To prepare polycrystalline $Y_1Ba_2Cu_3O_{7-\delta}$:Ag sample by the solid state reaction technique.

(ii) To develop a simple experimental technique to measure ac loss.

(iii) To assess the effect of electromagnetic radiation on the ac loss measurement.

(iv) To investigate the effect of intensity of laser radiation on the ac loss.

CHAPTER IV
EXPERIMENTS

4.1 Superconducting Specimen Preparation

The superconducting specimen, $Y_1Ba_2Cu_3O_{7-x}$:Ag, was prepared using the solid state reaction technique. This technique involves mixing of yttrium oxide (Y_2O_3), barium carbonate ($BaCO_3$), copper oxide (CuO), and silver (Ag) powder followed by several high temperature heat treatments. The heat treatments thermally accelerate the reaction between the component oxides and enhance the formation of superconducting phase. The superconducting sample thus prepared was ground to a powder (sieved at 75 microns) and mixed with silver powder (1-3 micron size). Calculated amounts of both powders were ground in an agate mortar until a uniform consistency was obtained. The sample was pressed into a 3/4 inch diameter pellet, placed in a small alumina crucible, and encapsulated in quartz. The quartz capsule was heated for 50 hours at 1000°C and allowed to cool slowly to about 375°C at a rate of 1°/min within the furnace. After the heating cycle was completed, the pellet was removed from the capsule, and the Meissner effect was measured by the magnetic pendulum method [48]. The deflection was found to be around 4.16 mm. Next, the 123:Ag pellet was ground into a powder and pressed into three new pellets with a 3/4 inch diameter and a weight of about 3 grams. The pellets were sintered simultaneously for 15 hours at 915°C and

were cooled for 8 hours to about 200°C. A constant flow of oxygen was maintained inside the furnace at a rate of 10 cubic feet per hour (c.f.h.) during the heating and cooling periods. The purpose of sintering and cooling the material in an oxygen atmosphere was to control the crystal structure of the material. After sintering, the pellets were evaluated using the magnetic pendulum. The pellet with the largest deflection was tested for current density and critical temperature. The results are shown in Table 1.

Table 1

Results of Encapsulation and Sintering

Pellet No.	silver (%)	Deflection(mm)	$J_c(A/cm^2)$	$T_c(^oK)$
1	20	4.21	125.8	76.5
2	20	6.04	128.5	77.2
3	20	5.97	130.2	79.0

Additional encapsulations were made by adding 20% of the silver to the 123:Ag at different atmospheric pressures. The results are tabulated in Table 2. Samples E-3 through E-6 were heated at 1000°C for 50 hours and allowed to cool slowly to about 350°C at a rate of 1°/min within the furnace. After cooling, the pellets were removed from the capsules and measured for deflection using the magnetic pendulum. The pellets were then ground and sintered at 915°C and cooled for 8 hours to 200°C. The oxygen flow was maintained within the furnace at 10 c.f.h. during the heating and cooling periods. All samples exhibited the Meissner effect when cooled to liquid

nitrogen temperature. The sintered samples, E-3 to E-6, were measured for current density and transition temperature. The results are tabulated in Table 2.

Table 2

Meissner Effect, Current Density, and T_c of Samples E-3 through E-6.

Sample No.	Oxygen atm	Deflection before sintering (mm)	Deflection After sintering (mm)	J_c (A/cm^2)	T_c (°K)
E-3	1	2.49	6.21	71	85
E-4	2	1.51	6.58	132	87
E-5	3	4.02	4.20	180	90.1
E-6	4	1.62	5.83	125	88.5

4.2 AC Loss Measurement

Figure 4.1 shows a schematic of the ac loss measurement experimental setup. This technique employs a specimen with four-point contacts, as shown in Figure 4.2. A rectangular bar was cut from the E-5 sample and indium contacts were applied. An ac current of varying frequency f, which was produced by a sine wave generator, was allowed to flow through the two external leads of the specimen. An EG&G PARC Model 5209 lock-in amplifier was used to measure the alternating current losses in the superconductor. A Realistic Model QA-622 stereo amplifier was used to keep

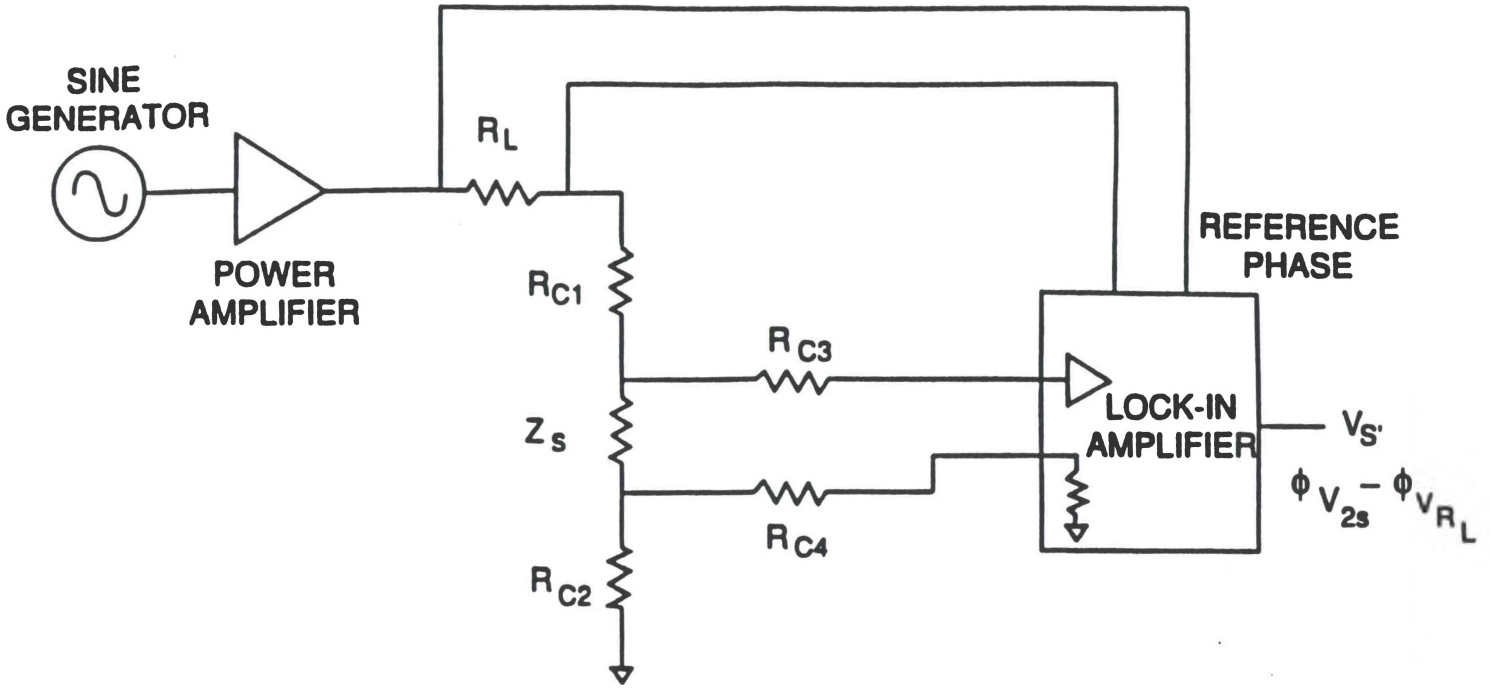

Figure 4.1 Schematic of the ac Loss Measurement Setup.

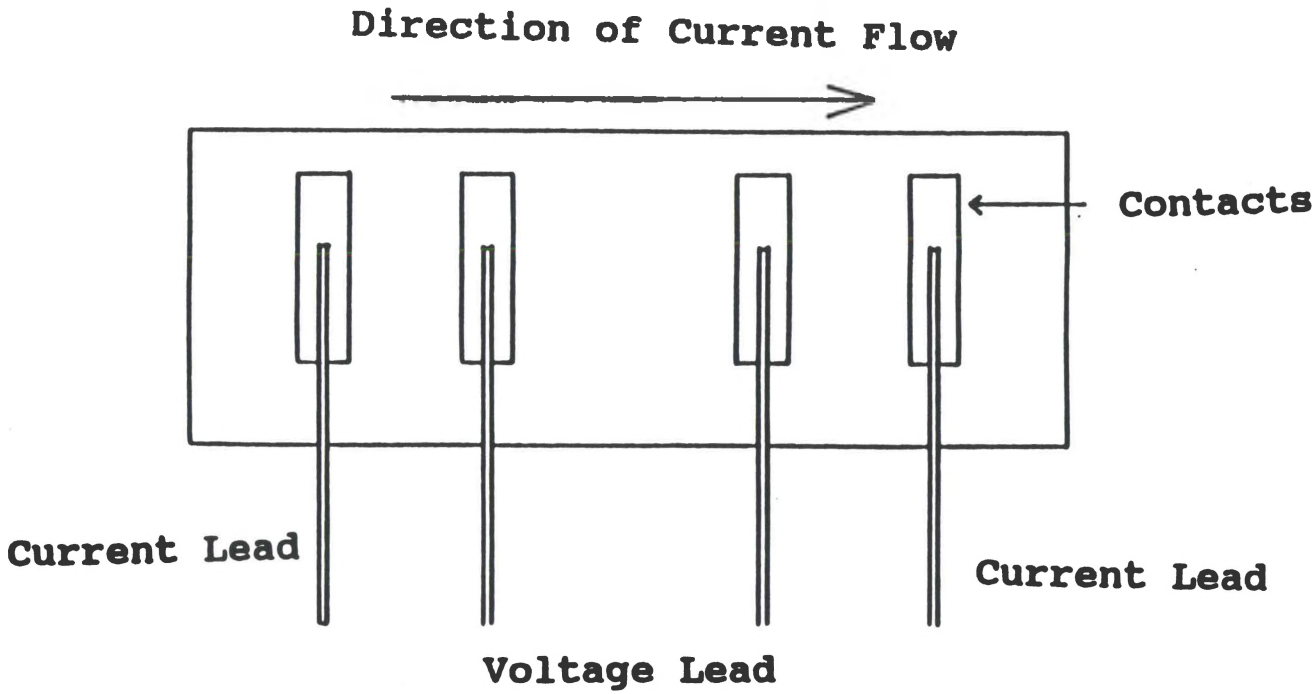

Figure 4.2 Diagram of the Four Point Probe Technique.

the current constant throughout the experiment. A non-inductive load resistance of 8.246 ohms was used as the output load; the purpose of the load resistance was to stabilize the flow of current. If the current source were attached directly across the sample, the noise level would be significant and the current would not be constant.

The sample was placed in a sample holder with good thermal insulating properties. Electrical connections were made by soldering one end of a thin silver wire to the indium paste and the other end to a thick silver wire. To avoid any chance of damaging the sample, a low melting point Ag-Pb-Sn solder was used.

In the first phase of the experiment, an ac current of 107 mA was passed through the outer two leads of the sample. To maintain this current, a peak-to-peak voltage of 2.5 V was kept constant during the measurement. A Philips Model PM-3232 oscilloscope was used to observe this voltage waveform. While keeping the current constant, the frequency of the signal was varied and the voltage drop, V_S, across the inner two leads was measured using the lock-in amplifier. The phase difference, ϕ, between the current and the voltage was also measured. The impedance, Z, is equal to the ratio of V_S to I_{rms}. The measured impedance, Z, is comprised of a resistive component, $|Z|\cos\phi$, and a reactive component, $|Z|\sin\phi$. The power loss originated with the resistive component and was calculated from the expression $P=I^2_{rms}R$. The ac loss data presented in this study was obtained by dividing the power loss by the cross sectional area of the specimen.

4.3 Effect of Electromagnetic Radiation

4.3.1 Effect of ambient illumination and HeNe laser

Another set of experiments were performed to investigate the effect of electromagnetic radiation on ac losses. The specimen was isolated from ambient illumination by covering the sample holder with a black box, and measurements were made as before. Subsequently, another experiment was performed in which the specimen was exposed to ambient illumination in addition to being illuminated with a 3 mW HeNe laser at a wavelength of 632.8 nm.

4.3.2 100 Hz ac Losses with Various ac Currents

In the second phase, another set of experiments were conducted to observe the relationship between current and ac losses. To measure ac losses, the frequency of the ac signal was kept constant at 100 Hz and the ac current was varied from 64 mA to 171 mA by changing the oscillation level of the lock-in amplifier. In addition, a voltage-current (V-I) relationship was obtained for the superconducting sample. The ac loss was calculated for different voltage and current values at 100 Hz. The sample was additionally irradiated with a HeNe laser to observe the effect of electromagnetic radiation on ac loss of the superconductor.

4.3.3 Effect of Laser Intensity on ac Losses

A set of experiments were performed using a Spectra-Physics Model 166 Argon-ion laser. The schematic of the set-up is shown in Figure 4.3. This laser operates in a continuous (CW) mode and has two strong transition lines, 488 nm and 514.5 nm. The Green line (514.5 nm) was used to illuminate the sample. In this experiment, a rectangular bar was cut from the silver doped 123 (E-4R) sample. While the sample was being mounted, a mechanical shutter was used to block the laser beam. Mirrors M1 and M2 were used to focus the beam on the center of the sample. A Newport Research Model 815 power meter recorded the power of the beam and a Newport Model 150 Neutral density filter (NDF) varied the intensity of the laser output; the NDF could attenuate the beam by almost 95%. The beam diameter was measured and the intensity was calculated. Eight different sets of measurements were conducted with various intensities for the ac frequencies of 1 KHz, 5 KHz, and 10 KHz. The ac loss was calculated in each case. All the measurements were conducted at the liquid nitrogen temperature.

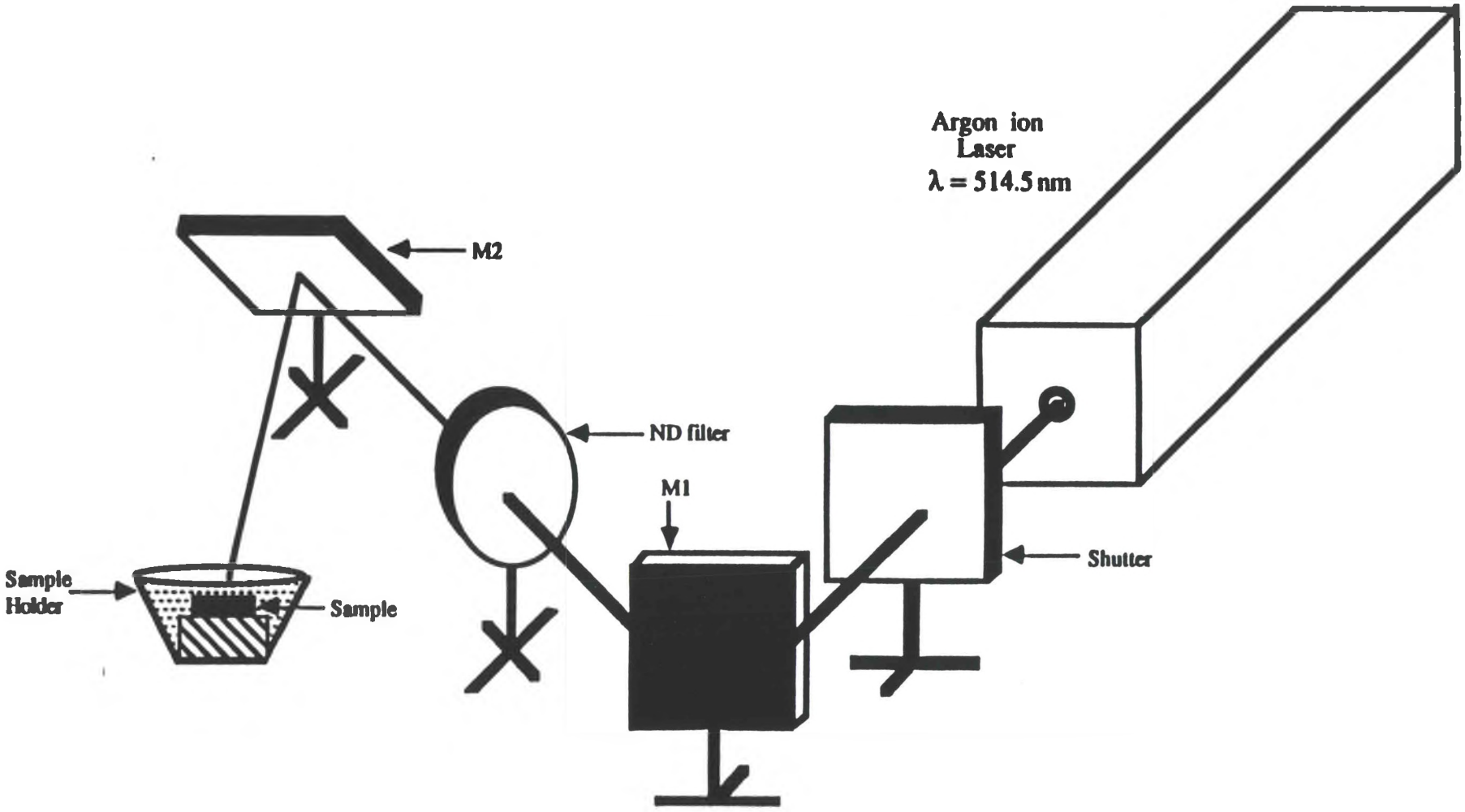

Figure 4.3 Experimental Setup to Measure the Intensity Dependence of ac Loss.

CHAPTER V
RESULTS AND DISCUSSION

5.1 AC Losses in High-T_c Superconductors

The nonresistive transmission of electricity below the critical temperature (T_c), critical current (J_c), and critical magnetic field (H_c) is limited to only dc currents. The temperature-dependent resistive loss of ac currents below these critical points is a well-documented characteristic of superconductors. There are numerous factors that are known to affect ac resistivity. These factors include the presence of normal electrons below the critical points; the motion of fluxoids in type II superconductors; eddy current losses due to cladding materials, and temperature; and the microstructure of the superconducting materials. In effect, ac losses can be classified in two broad categories: (1) intrinsic losses which arise due to the electronic state or order of the materials and (2) extrinsic losses [49-51] arising from factors such as in the microstructure, cladding, etc., that originate from the processing of the material. Both types of losses are important to the development of high temperature superconducting materials for applications such as power transmission, motors, generators, and other power equipment.

Intrinsic ac loss is generally explained on the basis of the two fluid model originally proposed by Gorter and Casmir [52]. The model postulates the existence of two kinds of electrons--superelectrons, or superconducting electrons (n_s), and normal (n_n) electrons--below the critical temperature. Superelectrons are able to pass through the material without resistance, not encountering any collisions. But, normal electrons can be scattered; thus, like conduction electrons in a normal metal, they experience resistance. The fraction of superelectrons, n_s, increases as the temperature is lowered below the critical temperature and approaches unity at absolute zero. As the temperature increases, a few superelectrons begin to behave as normal electrons; upon further raising the temperature, the proportion of normal electrons increases. These normal electrons, n_n, are believed to interact with the ac field and lattice, giving rise to ac resistivity and power loss. Intrinsic ac loss is temperature dependent and is explained by using an assumption of the two fluid model; that is, since the number of normal electrons is larger near the T_c, higher ac losses occur around this critical point as compared to a temperature near absolute zero.

The experimental technique to measure ac loss was discussed in the previous chapter. As mentioned earlier, an ac current, I_{rms}, of varying frequency was allowed to flow through the two external leads of the specimen. The voltage drop across the two inner leads and the phase difference between the current and the voltage were also measured. Thus, the value of the impedance was obtained by taking the ratio of voltage to ac current.

The impedance, measured in mΩ as a function of frequency, is shown in Figure 5.1. It is noted that, as frequency f increases, the impedance, z, increases linearly over the entire frequency range of the measurement. A regression analysis revealed that the impedance, z, is related to frequency as expressed by equation (5.1) with a correlation coefficient of r = 1.000

$$z = 5.51f \qquad (5.1)$$

Impedance is comprised of both resistive and reactive components. The resistive loss was calculated using the impedance and phase angle data. After dividing the resistive loss by the cross-sectional area of the specimen, the ac loss, expressed in $\mu w\ cm^{-2}$, is measured at 77.2 K; this is represented by the open triangles Figure 5.2. The ac loss, P, shows a nonlinear frequency dependence. Analytically, the relationship between ac loss and frequency is expressed by equation (5.2):

$$P = 2.85f + 3.63f^2 \qquad (5.2)$$

The ac loss behavior is consistent with the data reported in the literature concerning $Bi_2Ca_2Sr_2Cu_3O_{10}$ tapes by Orehotsky et al. [51]. The frequency dependent loss may be rationalized with the two fluid model. It is also believed that the normal electrons in alternating fields collide with the lattice, giving rise to resistivity and resulting in ac losses. Besides the two fluid model, one could explain the ac loss in the way that the current is changing, an electric field must be developed to accelerate the electrons and because of electrons' inertial mass, the supercurrent does not rise instantaneously but only at the rate at which the electrons accelerate in

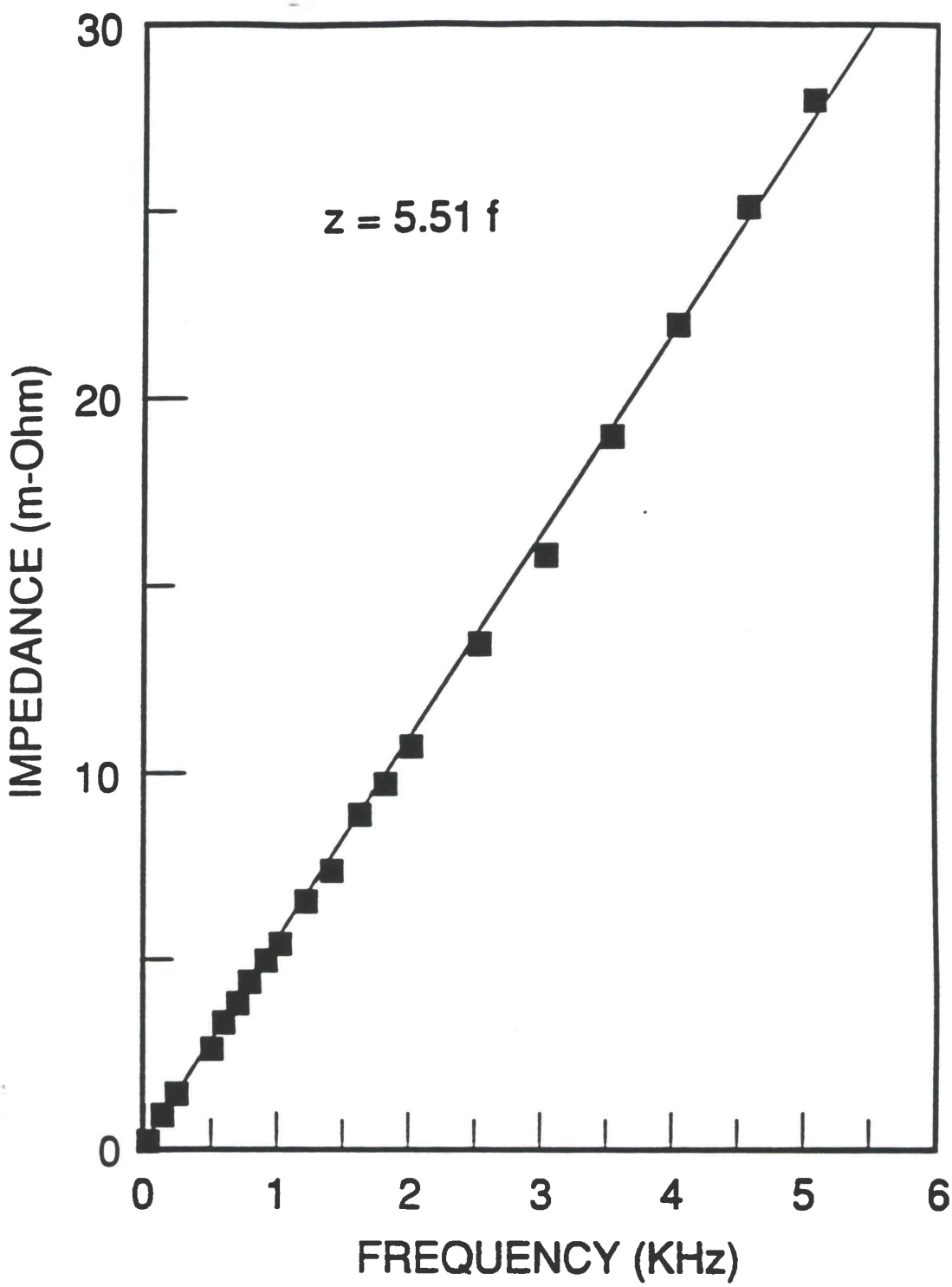

Figure 5.1 Impedance of a $Y_1Ba_2Cu_3O_{7-\delta}$ Ag superconductor at 77.2K as a function of frequency.

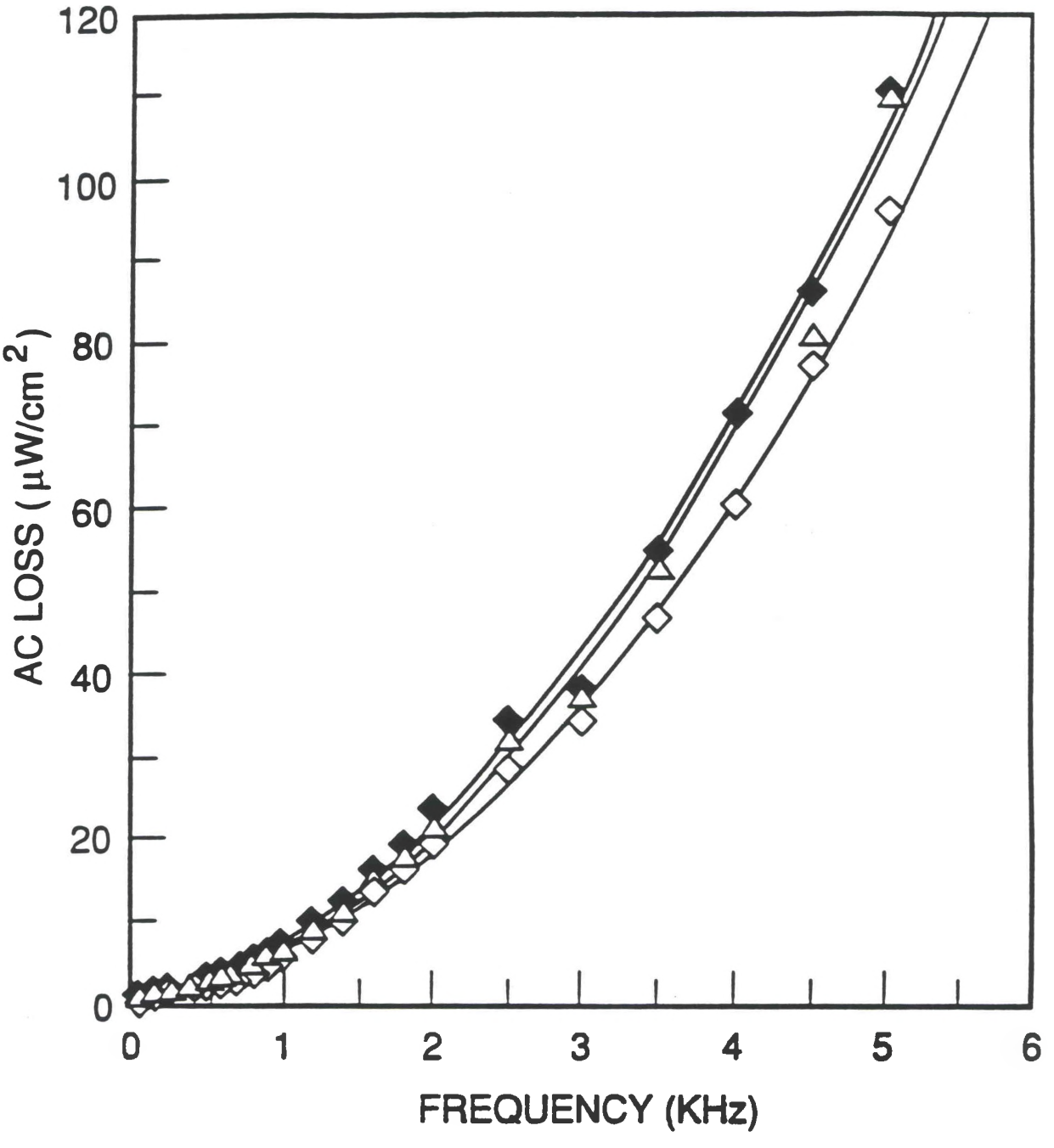

Figure 5.2 AC loss of $Y_1Ba_2Cu_3O_{7-\delta}$:Ag superconductors; ◆ exposed to HeNe, Δ ambient illumination, ◇ isolated.

the electric field [11]. It is thus believed that the supercurrent lags behind the electric field because of the inertia of the superelectrons in the alternating field. Since, in this case, the field is not constant, some of the current will be carried by the normal electrons and introduce resistance.

5.2 Effect of Electromagnetic Radiation on ac Losses

The interaction of electromagnetic radiation with superconductors has received considerable attention since the discovery of superconductivity [53,54]. At very low frequencies (far IR), superconductors are highly reflective. However, as the frequency increases and the energy of the electromagnetic radiation becomes comparable to the gap in the energy spectrum or to the energy of the Cooper pair, an interaction starts and the superconductors begin to absorb the incident electromagnetic radiation. The phenomenon allows one to determine the energy of the Cooper pair by using optical spectroscopy techniques. The interaction also leads to the de-pairing of superconducting electrons and, thus, to the generation of normal electrons sometimes referred to as quasi-particles. The energy of visible optical radiation ($\cong$ 2 - 5 eV) is much higher than the energy of a Cooper pair even in high-T_c superconductors ($\cong 10^{-2}$ - 10^{-3} eV). Therefore, visible electromagnetic radiation is highly energetic to interact with superconductors and to increase the fraction of normal electrons (quasi-particles). It is these normal electrons that may affect ac losses.

Figure 5.2 also shows the effect of electromagnetic radiation on ac losses. When the specimen was isolated from ambient illumination, the ac losses, represented by open diamonds in Figure 5.2, decreased over the

entire frequency range. The best fit of the experimental data is given by equation (5.3):

$$P = 3.02f + 3.15f^2 \qquad (5.3)$$

As expected, the coefficients of equations (5.2) and (5.3) are different; however, their physical interpretation is not quite clear at the present time. The differences in the ac losses of the specimen when isolated or exposed to ambient illumination appear to have increased with frequency. Thus, another experiment was performed to determine the effect of electromagnetic radiation on ac losses. In this experiment, the specimen exposed to ambient illumination was additionally irradiated with a 3 mW HeNe laser. Again, in this case, the ac losses increased as compared to the specimen illuminated by ambient light, as shown by the solid diamonds in Figure 5.2. However, the difference in ac loss as a function of frequency between these two seems to be smaller. An analytical expression for this effect is given by

$$P = 3.96f + 3.50f^2 \qquad (5.4)$$

Several different groups [55,56] have measured the ac losses in type II superconductors, and their results at low frequencies are of the form

$$P = af + bf^2 \qquad (5.5)$$

Equations (5.2) - (5.4) are very much consistent with equation (5.5). At very low frequencies, ac losses increase linearly with frequency, and, with the increase of frequency, ac losses increase in a non-linear fashion. At low frequencies, losses are attributed to flux creep and hysteresis, and, in the

intermediate frequency range (≥ 500 Hz upto a few MHz), the losses in superconductors are due largely to the hysteretic motion of vortices through the material. In fact, hysteresis losses are expected to be more dominant in the ac loss mechanism. These losses originate because of the irreversible magnetization of superconductors and are strongly dependent on the maximum amplitude of ac fields and currents relative to the critical values. The design of ac power systems employing superconductors is influenced greatly by these considerations. It can also be argued that the two most important factors determining ac losses in superconductors are the surface conditions and the bulk pinning force. To further explain ac loss in superconductors, theoretical studies related to the ac loss mechanism need to be developed. The BCS theory explains how superconductivity works but it does not discuss the mechanism of ac loss. Also, the review of literature does not provide enough information to explain ac loss in depth.

The I-V characteristics of the sample measured at a frequency of 100 Hz at 77.2 K are shown in Figure 5.3. The I-V curve obeys Ohm's law; that is, with an increase of current, the voltage across the sample increases linearly. This result is quite consistent with the measurement made by S. Kagoshima et al. [57], whose results also indicate a similar shape of the I-V curve and suggest that temperature is the predominant factor determining shape. It is expected that the segments in a superconducting state connected serially to a normal state turn into normal states under an increasing current. As a result, the overall resistance of the sample, as well as its ac losses, are increased.

Figure 5.4 shows the ac loss at 100 Hz as a function of the ac current under ambient and HeNe laser illuminations. The ac loss shows a non-

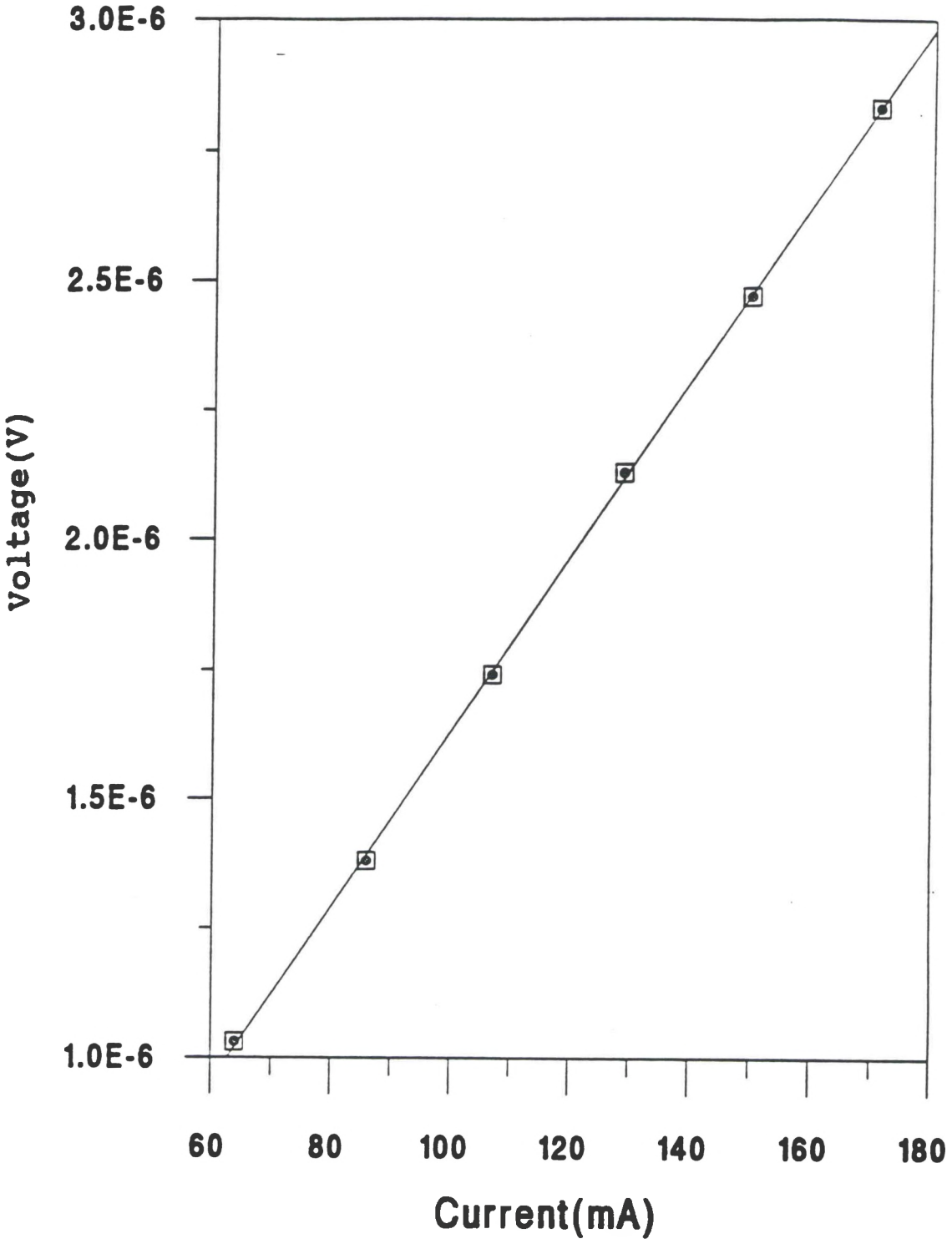

Figure 5.3 I-V Characteristics of $Y_1Ba_2Cu_3O_{7-\delta}$:Ag superconductor at a frequency of 100 Hz without illumination.

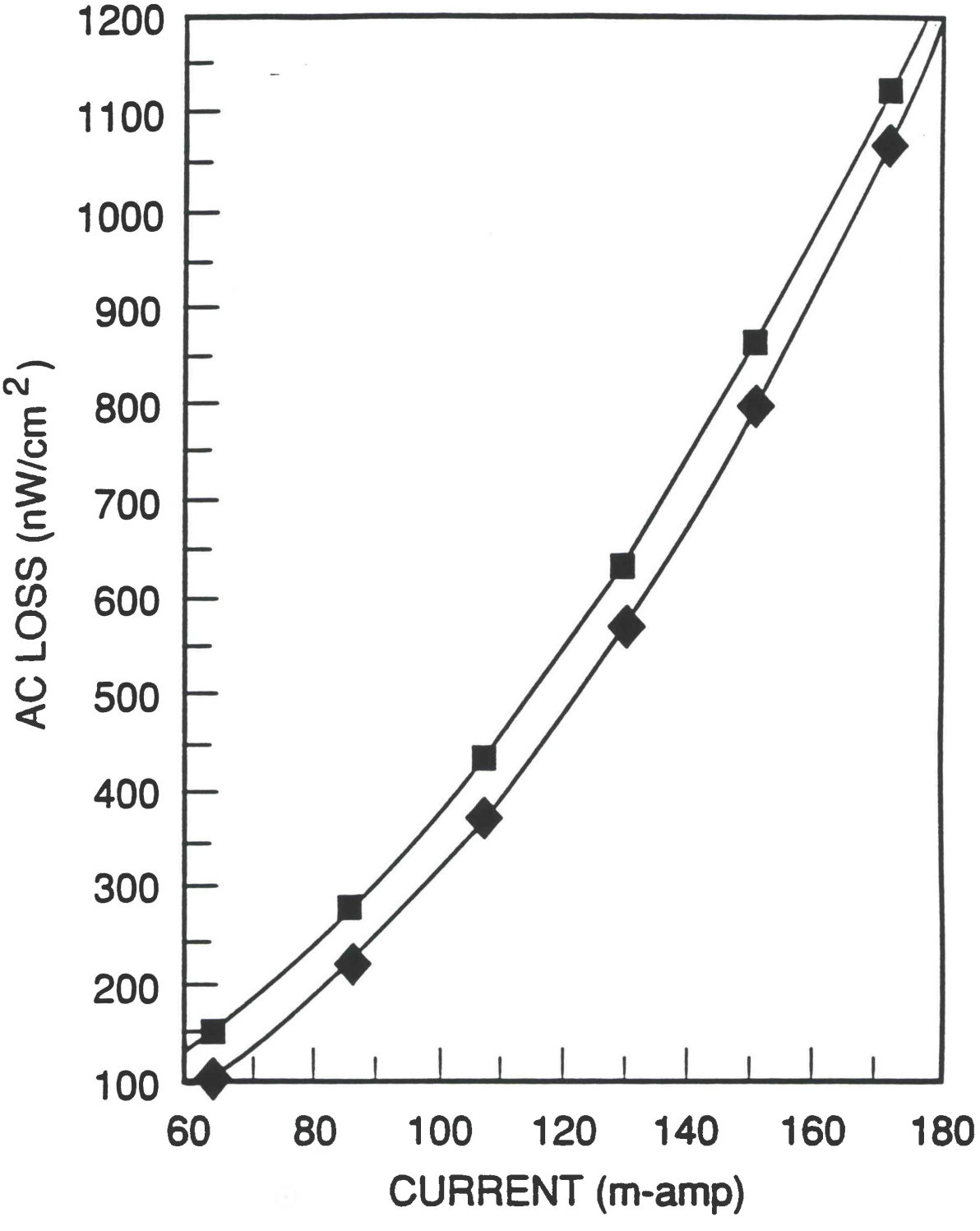

Figure 5.4 AC losses in $Y_1Ba_2Cu_3O_{7-\delta}$ Ag superconductor at 100 Hz; ◆ ambient illumination, ■ ambient plus He-Ne illumination.

linear relationship with current. Irradiating the specimen with the HeNe laser again increased the magnitude of the ac loss, and the two curves of Figure 5.4 are virtually parallel.

The effect of electromagnetic radiation on ac losses is believed to be related to the generation of additional charge carriers. It was stated earlier that the energy of superconducting electron pairs (10^{-2} - 10^{-3} eV) is much lower than that of ambient light (2 -5 eV) and of HeNe lasers ($\cong$ 1.96 eV). These highly energetic radiation sources break the superconducting pairs into normal charge carriers which then interact with the alternating field and the lattice, giving rise to an enhanced ac loss.

It is expected that ac loss will be dependent upon temperature and intensity as well as upon the frequency of electromagnetic radiation. Thus, an additional experiment was performed to assess the intensity dependence of ac loss in superconductors.

5.3 Intensity Dependence of ac Loss

The effect of electromagnetic radiation on ac losses in high-T_c superconductors, as reported earlier [58], prompted a further investigation of the intensity dependence of ac loss. By varying the power of an Argon-ion laser from 10 mW to 500 mW, ac losses at three different frequencies were measured, and the results are shown in Figure 5.5. Equations (5.6)-(5.8) represent the power dependence of ac losses at frequencies 1 KHz, 5 KHz, and 10 KHz (by solid squares, open diamonds and solid diamonds, respectively) :

$$E_1 = 316.743 + 0.0085\ P_o \quad (5.6)$$

$$E_5 = 339.462 + 0.0083\ P_o \quad (5.7)$$

$$E_{10} = 364.848 + 00.49\ P_o \quad (5.8)$$

where P_o is the output power of the Argon-ion laser.

After measuring the beam diameters, the intensity dependence of ac loss was plotted with error bars, as is shown in Figure 5.6. Three different equations with frequencies 1 KHz, 5 KHz, and 10 KHz, representing the best fit of the experimental data, are respectively presented by equations (5.9) - (5.11).

$$W_1 = 316.487 + 0.336\ I \quad (5.9)$$

$$W_5 = 339.182 + 0.333\ I \quad (5.10)$$

$$W_{10} = 364.675 + 0.199\ I \quad (5.11)$$

where I is the corresponding intensity of laser radiation. In this case, ac loss at a frequency of 1 KHz, 5 KHz, and 10 KHz are respectively represented by open squares, solid triangles and open triangles. The ac loss at zero power and/or zero intensity implies that the specimen was isolated from laser radiation but illuminated by ambient light. From Figures (5.5) and (5.6), it is clear that ac loss due to ambient illumination is less compare to laser radiation, which is consistent with the results reported earlier.

AC losses in superconductors increase linearly with the intensity of laser radiation at the three different frequencies. The intercepts and the slopes in all three cases are different. From the intercept, it is quite evident

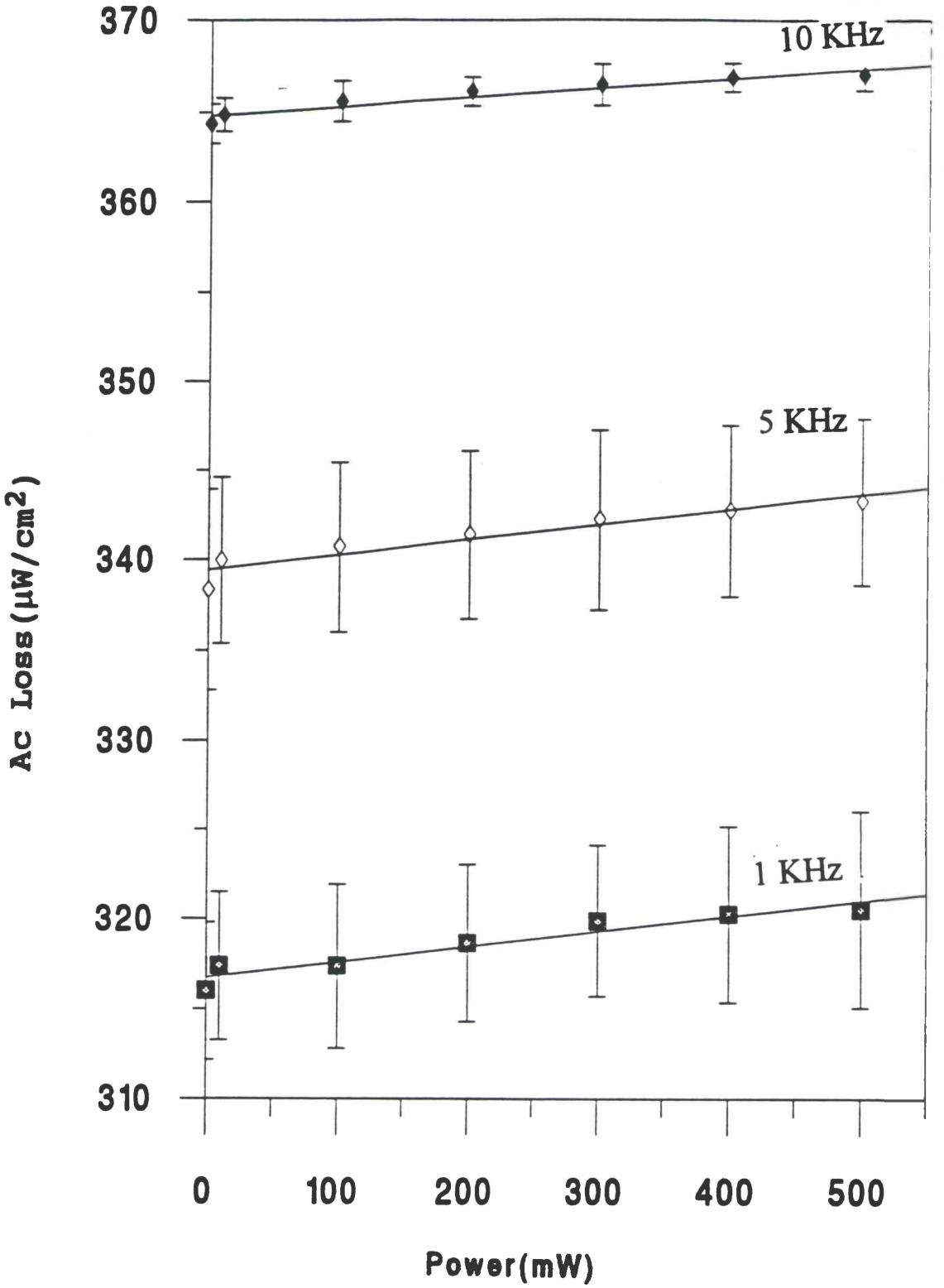

Figure 5.5 Variation of ac loss of $Y_1Ba_2Cu_3O_{7-\delta}$:Ag superconductor with the power of Argon-ion laser.

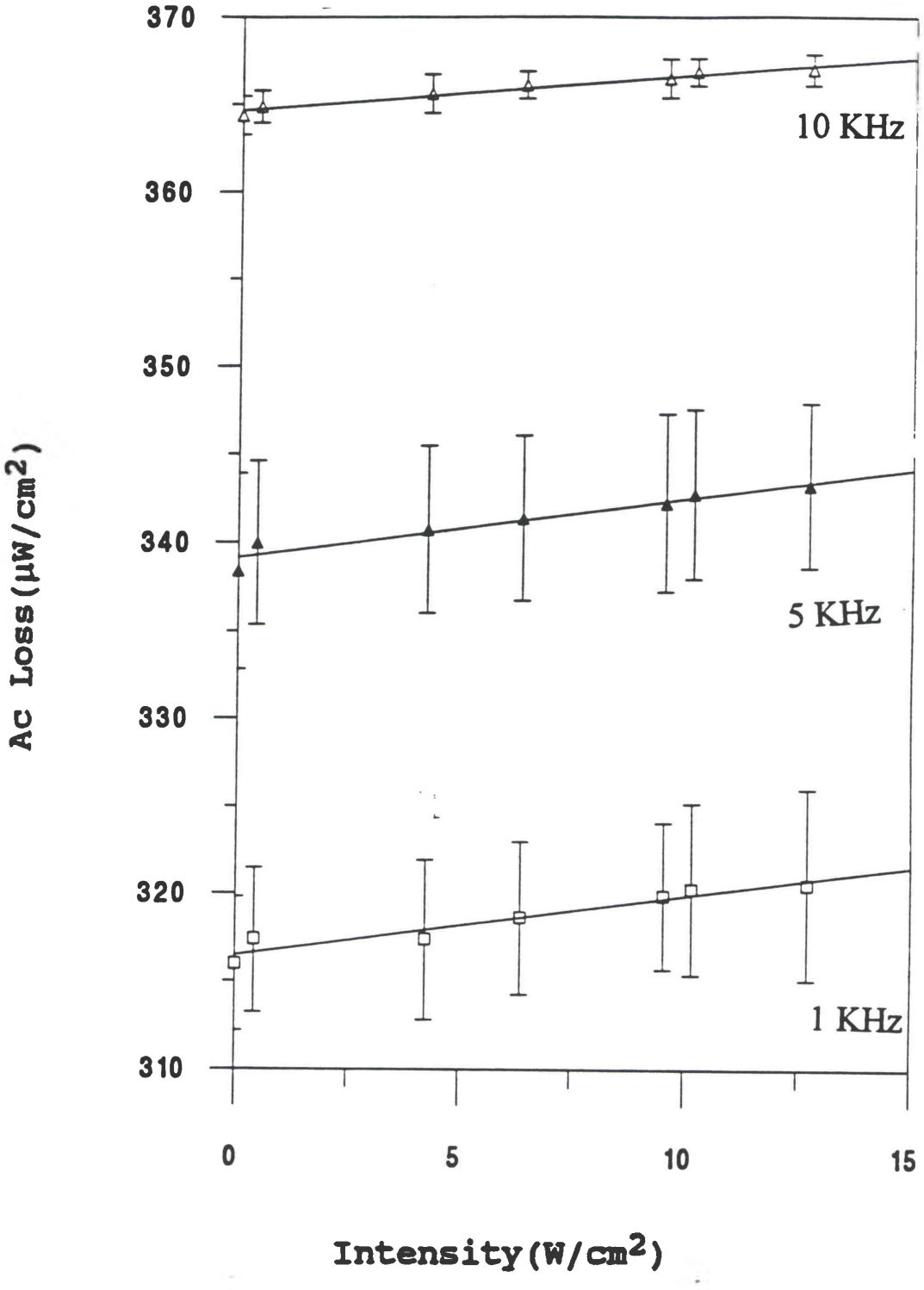

Figure 5.6 Effect of intensity of laser radiation on ac losses of $Y_1Ba_2Cu_3O_{7-\delta}$:Ag superconductor.

that ac loss is frequency dependent, which is consistent with the data reported earlier. The slopes of the above equations decrease as frequency increases, indicating that, with the unit increment of laser power, there will be a smaller increase in ac loss at higher frequencies. Thus, from this result, it will be very reasonable to accept that, at higher frequencies, ac loss will be almost independent of laser radiation.

The enhanced ac loss in superconductors could be due to either the thermal (bolometric) or non-thermal responses of the specimen to the intensity of laser radiation. In the present investigation, the specimen was irradiated at a temperature less than the T_c; the non-thermal response appears to be the major factor to increase the impedance and, as a result, an increase in ac losses. It is expected that the superconducting pairs will be destroyed by the injection of photons and that the number of normal electrons (quasi-particles) will increase as a result. The origin of quasi-particles can be explained within the two fluid model, where the conductivity, σ, is written as

$$\sigma = N_n\sigma_n + N_s\sigma_s \qquad (5.12)$$

where N_n and N_s are the relative densities of the normal and the superconducting electrons and σ_n and σ_s are their respective conductivities. Thus, the generation of quasi-particles, N_n, increases at the expense of N_s due to the intensity of laser radiation.

In order to explain the data, the number of quasi-particles corresponding to different input power levels of an Argon-ion laser was calculated. The maximum number of quasi-particles that can be created as a

result of a single photon absorption is roughly $g = \frac{2h\nu}{2\Delta(0)}$, where hν is the energy of a single photon and $2\Delta(0)$ is the energy gap in a superconductor. Following Friedl et al. [59], the value for $2\Delta(0) \approx 5K_BT_c$ and, for an Argon-ion laser (λ = 514.5 nm), is $2h\nu = 4.83$; the estimated number of quasi-particles due to a single photon absorption is ~ 120. Thus, the total number of photons for different input power levels was calculated using N = Po / hν, where P_o is the output power of the laser. It is believed that these photons are responsible for generating quasi-particles in superconductors. Figure 5.7 shows that the number of quasi-particles increases linearly as laser radiation increases and thus enhances ac losses in superconductors.

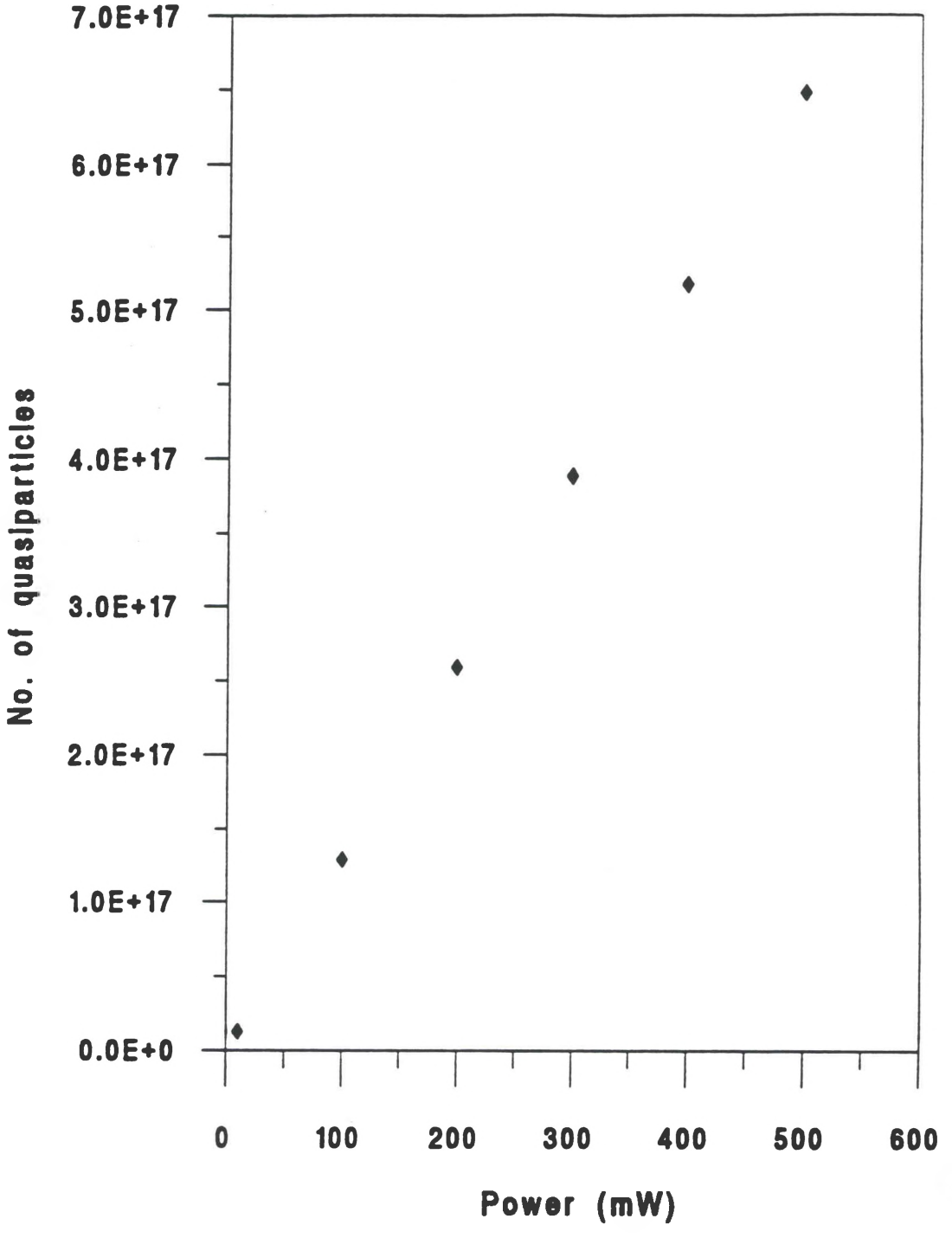

Figure 5.7 Quasi-particle generation due to the intensity of laser radiation.

CHAPTER VI
SUMMARY AND CONCLUSIONS

A simple experimental technique was developed to measure ac losses in high-T_c superconductors. The system is comprised of a lock-in amplifier, an oscilloscope, and a stereo amplifier. In order to determine the voltage drop across the sample, the amplifier provided an alternating current through the sample. The lock-in amplifier served to measure the voltage drop and the phase difference between current and voltage and also altered the frequency of the ac current. It was found that impedance increases linearly with the frequency of ac current. The resistive component, which is the real part of the impedance, was calculated to obtain the dissipative power of the specimen. Thus, ac loss was determined by dividing the dissipative power by the specimen cross sectional area. This ac loss increased in a non-linear manner with frequency.

The effect of electromagnetic radiation on ac losses was observed by isolating the specimen from ambient light. To confirm this effect, an experiment was performed in which the specimen was irradiated with a HeNe laser. In the former case, ac losses were found to be lower as compared to ambient illumination over the entire frequency range. The results were explained according to the two fluid model of superconductivity. The number of normal electrons increases at the expense of the superconducting electrons; as a result, ac losses were found

to increase. A current-voltage relationship of the superconducting specimen was established by varying the current and measuring the resulting voltage drop at a frequency of 100 Hz. The voltage drop varied linearly with the ac current. The ac losses were also measured at a frequency of 100 Hz with varying currents both with ambient light and with HeNe laser illumination. In this case, it was found that ac loss increased due to HeNe laser illumination.

Subsequently, another experiment was performed to investigate the effect of laser intensity on ac losses in superconductors. An Argon-ion laser with a wavelength of 514.5 nm and varied intensities was used to irradiate the specimen. ac loss was found to increase with the intensity of laser radiation. It was determined that, in the superconducting state, quasi-particles were generated due to the absorption of photons and, as a result, ac losses increased.

Although superconductors do not exhibit zero resistivity to alternating currents, they do have a much lower ac resistance below T_c than above and their impedance increases with frequency. This increase in ac loss is proportional to the square of the frequency. In this case, a comparison of the experimental data with the literature was in good agreement. But a review of the literature has shown that the theoretical information regarding ac loss is inadequate to explain the ac loss mechanism.

Thus, the above discussion can be summarized in the way that this investigation has developed and demonstrated (a) a relatively simple technique to measure ac losses in superconductors, (b) to measure the

current-voltage relationship of a superconductor, (c) to determine the effect of electromagnetic radiation on ac losses, and (d) to study the intensity dependence of ac loss in superconductors.

CHAPTER VII
RECOMMENDATIONS FOR FUTURE WORK

Based on the work performed in this thesis, a number of future studies can be recommended. Some measurement techniques can also be modified and implemented to improve upon the existing data.

One problem encountered in the measurement of ac loss at high frequencies was the unavailability of proper equipment. It would be interesting to measure ac loss at a microwave or higher frequency range since superconductors have the potential to be used as microwave and IR detectors. To implement this measurement, a lock-in amplifier workable at this frequency region should be used. Also, a GHz impedance analyzer could be employed to perform this experiment. Another drawback to the existing experimental setup is the stereo amplifier; the present amplifier does not maintain the current at a constant high frequency. The waveform, as observed by the oscilloscope, was distorted at freqencies above 40 KHz, which is the result of the ac current variation caused by the amplifier. Thus, one can improve the present ac loss measurement setup by using a better lock-in amplifier and stereo amplifier.

Currently, samples are prepared for ac loss measurement by cooling them to liquid nitrogen temperature in a simple styrofoam sample holder. To maintain a constant level of liquid nitrogen, one must intermittently add

liquid nitrogen. It is possible to redesign the cooling system in order to ensure a constant level of liquid nitrogen. In addition, it would be interesting to further investigate the effect of electromagnetic radiation on ac losses in superconductors while keeping a constant level of liquid nitrogen in order to obtain more accurate data. Adding a cryostat and a temperature controller would minimize the sources of error and give flexibility to measuring the temperature dependence of ac loss.

Other high temperature superconducting materials such as $Tl_2Ba_2Ca_1Cu_2O_8$ and $BiSr_2Ca_1Cu_2O_{8+\delta}$ should be fabricated and prepared for ac loss measurement. A single crystal of silver doped and sodium doped $Y_1Ba_2Cu_3O_{7-\delta}$ could also be used for investigation.

One could also measure relaxation time, which is the time for recombination of quasi-particles to form Cooper pairs. The work of this thesis demonstrates that the intensity of laser radiation can enhance ac loss and introduce a resistive state in superconductors. The superconducting state is restored by isolating the specimen from the electromagnetic radiation. Thus, by using a laser, superconducting films could be used as an optical switch.

APPENDIX-A

Flux Creep and Flux Pinning

The large relaxation effect that causes a decay of magnetization and of the persistent current is called flux creep. It is a thermally activated process which is mainly due to a combination of low pinning potentials and of a temperature relatively higher (i.e. 77K) than that at which these materials are intended to be used. Stated in simple terms, the creep is the result of the jumping of trapped-flux lines from one pinning region to another. Researchers have found flux creep in various high-T_c ceramic superconductors (HTS) to be a major challenge since their coherence lengths are extremely small, with values on the order of 10Å; as a result, flux vortex migration can easily take place. In principle, the creep rate can be decreased by increasing the pinning potential. Even though the origin of pinning in HTCS is still the subject of considerable discussion, the main pinning mechanisms are being recognized as intrinsic pinning [60], pinning by extended defects such as intergrowths and boundaries [61], pinning by second phase inclusions [62], or pinning by point or columnar defects [63,64]. Neutron irradiated 123 single crystals have produced J_c values on the order of 6×10^5 A/cm^2, an improvement of almost two orders of magnitude over un-irradiated crystals. This remarkable development is believed to be caused by inducing point defects with sizes equal to the coherence length. In a thin film of 123 material, the natural existence of numerous screw dislocations and columnar holes is believed

to be responsible for providing effective pinning sites. The achievement of a high-J_c in single crystals indicates that it is possible to increase the J_c values in bulk or tape polycrystalline 123 materials by eliminating all the weak links and cracks; and by aligning the crystals. In other words, processing techniques should be optimized to produce the necessary concentration of flux pinning centers while eliminating weak link features. The use of HTSC materials for large-scale applications requiring high-J_c values will become possible only upon adopting high quality monolith or tape materials in place of the millimeter size single crystals. Since irradiation methods are not accessible to the manufacturing process, the development of processing methods to produce usefully shaped 123 material with the appropriate pinning sites is very important.

REFERENCES

1. P. Garoche and C. Noguera, "Breakdown of the BCS theory in the new high-T_c superconductors" MRS Anaheim Symp., CA., pp. 243 (1987).

2. S.A. Wolf and V.Z. Kresin, editors, Novel Superconductivity: proceedings of the International Workshop on Novel Mechanisms of Superconductivity, Berkeley, California, (Plenum Press, New York, 1987).

3. J.G. Bednorz and K.A. Müller, "Superconductivity at 93K in a new mixed-phase Y-Ba-Cu-O compound at ambient pressure," Z. Phys. B64, 189 (1986).

4. M.K. Wu, J.R. Ashburn, C.J. Torng, P.H. Hor, R.L. Meng, L. Cao, Z.J. Huang, Y.Q. Wang, and C.W. Chu, "Superconductivity at 93 K in a New Mixed-Phase Y-Ba-Cu-O Compound at Ambient Pressure," Phys. Rev. Lett., 58, 908, 1987.

5. H. Maeda, Y. Tanaka, M. Fukutomi, and A. Toshihisa, "A New High-T_c Oxide Superconductor Without a Rare Earth Element," Jpn. J. Appl. Phys. 27, L209-L210, 1988.

6. Z.Z. Sheng and A.M. Harman, " Bulk Superconductivity at 120 K in the Tl-Ca/Ba-Cu-O System," Nature 332, 138 (1988).

7. B.D. Josephson, "Possible new effects in superconductive tunneling," Phys. Lett. 2, 251-53, 1962.

8. B. Kumar, "Magnetic Energy Storage Devices for Small Scale Applications," IEEE AES Systems Magazine, p.12, November 1992.

9. L.F. Schneemeyer, E.M Gyorgy, and J.V. Waszczak, "Magnetic characterization of rare-earth barium cuprate superconductors," Phys. Rev. B36, 8804 (1987).

10. B. Kumar, T.E. Gist, R.T. Fingens, and R.A. Flake, "Small magnetic energy storage systems using high temperature superconductors," Proc. of 26th Inter Soc. Eng. Conv., Boston, MA. pp. 538-543, (1991).

11. A.C. Rose-Innes and E.H Rhoderick, Introduction to Superconductivity, Pergamon Press, 1978, pp.14.

12. W. Meissner and R. Ochsenfeld, "Naturwissenschaften" 21, 787 (1933).

13. D. Fishlock, editor, A Guide to Superconductivity, Macdonald: London, 1969, pp.29.

14. Clarke, J., "Small-scale analog applications of high-transition temperature superconductors," Nature, 333, No. 6168, May 5, pp. 29, 1988.

15. Pippard, A.B., "Early Superconductivity Research (Except Leiden)," IEEE Trans. Magn., MAG-23, No.2, pp. 371, March, 1987.

16. London, F, Superfluids, Macroscopic Theory of Superconductivity, vol. 1, John Wiley & Sons, New York, pp. 27-52, 1950.

17. Karim, M. A., Electro-Optical Devices & Systems, Pws-Kent Pub.Co.,1990.

18. J.D. Doss, Engineer's Guide to High-Temperature Superconductivity, John Wiley & Sons, 1989, pp.84.

19. Buchhold, T.A., Cryogenics, 3, 141, 1963.

20. Buchhold, T.A., and Rhodenizer, R.L., IEEE Trans. Magnetics, MAG-5, pp. 429-33, 1969.

21. Buchhold, T.A., and Molenda, P.J., Cryogenics, 2, pp. 344-7, 1962.

22. Rocher, Y.A., and Septfonds, J., " Losses of Superconducting Niobium in Low Frequency Fields," Cryogenics 7, pp. 421, 1967.

23. Male, J.C., " Effect of trapped flux on ac loss measurements in superconductors," Cryogenics, 10, 381, 1970.

24. Melville, P.H., J. Phys. C: Solid St. Phys., 4, 2833-48, 1971.

25. Lewis, T.J., "High Field Electron Emission from Irregular Cathode Surfaces" J. Appl. Phys., 26, 1405, 1955.

26. Little, R.P., and Whitney, W.T., "Electron Emission Preceding Electrical Breakdown in Vacuum," J. Appl. Phys., 34, 2430, 1963.

27. Slivkov, I.N., "Initiation of Electrical Breakdown in Vacuum by Field Emission," Sov. Phys. Tech. Phys., 11, 249, 1966.

28. Miller, H.C., "Change in Field Intensification Factor β of an Electrode Projection (Whisker) at Short Gap Lengths" J. Appl. Phys., 38, 4501, 1967.

29. Kulik, I.O.,"The Josephson effect in superconducting tunnelling structures" Zh. eksp. teop. Fiz. Pis'ma, 3, 398, 1966.

30. Piel, H., Referred as Private Communication in Engineer's Guide to High-Temperature Superconductivity, James J. Doss, John Wiley & Sons, New York, 1989.

31. Aspnes, D.E., and Kelly, M.K., "Optical Properties of High-T_c Superconductors," IEEE J. of Quantum Electronics, 25, Nov, 1989.

32. Z. Schlesinger, R.T. Collins, D.L. Kaiser, and F. Holtzberg, "Superconducting Energy Gap and Normal-State Reflectivity of Single Crystal Y-Ba-Cu-O," Phys. Rev. Lett., vol. 59, p. 1958, 1987.

33. G.A. Thomas, J. Orenstein, D.H. Rapkine, M. Capizzi, A.J. Mills, R.N. Bhatt, L.F. Schneemeyer, and J.V. Waszczak, "Ba_2 Y Cu_3 $O_{7-\delta}$: Electrodynamics of Crystals with High Reflectivity,"Phys. Rev. Lett., 61, p. 1313, 1988.

34. I. Bozovic, D. Mitzi, M. Beasly, A. Kapitulnik, T. Geballe, S. Perkowitz, G. L. Carr, B. Lou, R. Sudharsanan, and S. S. Yom, "Vibrational spectra and lattice instabilities in the high-T_c Superconductors $YBa_2Cu_3O_7$ and $GdBa_2Cu_3O_7$," Phys. Rev. B, 36, No.7 pp. 4000,1988.

35. D.C. Mattis and J. Bardeen, "Theory of the Anomalous Skin Effect in Normal and Superconducting Metals," Phys. Rev., 111, p. 412, 1958.

36. F. Marsiglio, R. Akis, and J.P. Carbotte, "Thermodynamics in very strong coupling : A possible model for the high-T_c Oxides,"Phys. Rev. B, 36, p. 5245, 1987.

37. R.B. Laughlin, " The Relation Between High-Temperature Superconductivity and the Fractional Quantum Hall Effect," Science, 242, p. 525, 1988.

38. D.A. Bonn, J.E. Greedan,C.V.Stager, T. Timusk, M.G.Doss, S. L Herr, K. Kamaras, and D.B. Tanner, " Far-Infrared Conductivity of the High-T_c Superconductor $YBa_2Cu_3O_7$," Phys. Rev. Lett., 58, p. 2249, 1987.

39. R. Sobolewski, "Applications of high-T_c superconductors in optoelectronics," SPIE 1506 Micro-Optics 11, p. 25, 1991.

40. Rose, K., C.L. Bentin, and R.M. Katz, "Radiation Detectors," in Applied Superconductivity, 1, Newhouse, V.L., ed., Academic Press, pp. 267, 1975.

41. A. Hohler, D. Guggi, H. Neeb, and C. Heiden, " Fully textured growth of $Y_1Ba_2Cu_3O_{7-\delta}$ films by sputtering on $LiNbO_3$ substrates," Appl. Phys. Lett., 54, p. 1066, 1989.

42. S. G. Lee, G. Koren, A. Gupta, A. Segmuller, and C. C. Chi, "Epitaxital growth of $Y_1Ba_2Cu_3O_{7-\delta}$ thin films on $LiNbO_3$ substrates, " Appl. Phys. Lett., 55 , pp. 1261, 1989.

43. S. W. Cheong, S. E. Brown, Z. Fisk, R. S. Kwok, J. D. Thompson, E. Zirngiebl, and G. Gruner, " Normal-state properties of $ABa_2Cu_3O_{7-y}$ compounds (A=Y and Gd) : Electron-electron correlations, " Phys. Rev. B., 36, No.7,pp. 3913(1987).

44. K.L. Tate, R.D. Johnson, C.L. Chang, E.F. Hilinski, and S.C. Foster, " Transient laser-induced voltages in room-temperature films of $YBa_2Cu_3O_{7-x}$," J. Appl. Phys., vol. 67, p. 4375, 1990.

45. J.F. Scott, " Interpretation of photovoltaic pulses in normal $YBa_2Cu_3O_7$," Appl. Phys. Lett., 56, p. 1914, 1990.

46. K.L. Tate, E.F. Hilinski, and S.C. Foster, " Angle-dependent laser-induced voltages in room-temperature polycrystalline wafers of $YBa_2Cu_3O_{7-x}$," Appl. Phys. Lett., 57, p. 2407, 1990.

47. Chan, H. W. K and T. Van Duzer, " Josephson Nonlatching logic circuits," IEEE J. Solid state circuits," SC-12, No. 1, pp. 73, 1977.

48. A.S. Longo and B. Kumar, "Superconductivity Characterization by a Magnetic Pendulum," J. Superconductivity, 2(2), p 241, 1989.

49. J.R. Bumby, Superconducting Rotating Electrical Machines, Clanendon Press, Oxford, 1983, pp. 20.

50. J.F. Bussiere, M. Garber, and M. Suenaga, "AC losses in Nb_3Sn," IEEE Trans. on Magn., MAG-11, 324 (1975).

51. J. Orehotsky, K.M. Reilly, M. Suenaga, H. Hikata, M. Ueyama, and K. Sato, "AC losses in powder-in-tube $Bi_2Ca_2Sr_2Cu_3O_{10}$ tapes at power frequencies," Appl. Phys. Lett. 60, 252 (1992).

52. C.J. Gorter and H.G.B. Casimir, Phys. Z35, 963 (1934).

53. G. Burns, High-Temperature Superconductivity--An Introduction, Academic Press, 1992, p. 130.

54. S. Everding, Fabrication and Characterization of the High Temperature Superconductor $Y_1Ba_2Cu_3O_{7-x}$, M.S. Thesis, University of Dayton, 1989.

55. Murphy, J.H., Walker, M.S., and Carr, W.J., "Alternating field losses in a rectangular multifilamentary NbTi superconductor," IEEE MAG-11, (2), p. 313, 1975.

56. Kwasnitza, K., "ac Losses of Superconducting Composites with 8μm NbTi Filaments in a dc Magnetic Field with a Superimposed ac component at $1 \leq f \leq 500$Hz," Cryogenics 15, 732, 1975.

57. S. Kagoshima, S. Hikami, Y. Nogomi, T. Hirai, and K. Kubo, "Characterization of the High-T_c Superconductor Y-Ba-Cu Oxide--Critical Current and Crystal Structure-" Japn. J. of Appl. Physics, 26, No. 4, April, 1987, pp.L318-Z319.

58. B. Kumar and Kamal K. Das, "Effect of Electromagnetic Radiation on Alternating Current Losses in High-T_c Superconductors," J Appl. Phys.,73(12), June,1993, pp.8656.

59. B. Friedl, C. Thomsen, and M. Cardona, " Determination of the superconducting Gap in $RBa_2Cu_3O_{7-\delta}$," Phys. Rev. Lett., 65, 915 (1990).

60. M. Tachiki and S. Takahashi, " Strong Vortex Pinning in High-T_c Oxide Superconductors," Solid State Communication 70, 291 (1989).

61. Braginski, A. I., " Material constraints on electronic applications of oxide superconductors, " Proc. Int. Conf. on High Temperature Superconductors, Interlaken, Switzerland, Physica C 153, pp. 1598 (1988).

62. B. Ni., T. Munakata, T. Matsushita, M.Iwakuma, K. Funki, M. Takeo, and K. Yamafuji, " AC inductive measurements of intergrain and intergrain currents in high-T_c Superconductors, "Jpn. J. Appl. Phys. 27, pp.177 (1988).

63. L. Civale, A.D. Marwick, M.W. McElfresh, T.K. Worthington, A.P. Malozemoff, F. Holtzberg, J.R. Thompson, and M.A. Kirk, " Defect Independence of the Irreversibility Line in Proton-irradiated Y-Ba-Cu-O Crystals," Phys. Rev. Lett. 65, 1164 (1990).

64. L. Civale, A.D. Marwick, T.K. Worthington, M.A. Kirk, J.R. Thompson, L. Krusin-Elbaum, Y. Sun, J.R. Clem, and F. Holtzberg, " Vortex confinement by columner Defects in $YBa_2Cu_3O_7$ crystals : Enhanced Pinning at High Fields and Temperature,"Phys. Rev. Lett. 67, 648, (1991).